DOKUZ EYLÜL UNIVERSITY
GRADUATE SCHOOL OF NATURAL AND APPLIED SCIENCES

MEASURING THE TEMPERATURE DEPENDENT THERMAL CONDUCTIVITY OF MULTIWALL CARBON NANOTUBES BASED NANOLUBRICANTS BY 3 OMEGA METHOD

by

Abdulkareem ALASLI

March, 2018

İZMİR

MEASURING THE TEMPERATURE DEPENDENT THERMAL CONDUCTIVITY OF MULTIWALL CARBON NANOTUBES BASED NANOLUBRICANTS BY 3 OMEGA METHOD

A Thesis Submitted to the
Graduate School of Natural and Applied Sciences of Dokuz Eylül University
in Partial Fulfillment of the Requirements for Degree of Master of Science
in Mechanical Engineering, Energy Program

by

Abdulkareem ALASLI

March, 2018

İZMİR

M.Sc THESIS EXAMINATION RESULT FORM

We have read the thesis entitled **"MEASURING THE TEMPERATURE DEPENDENT THERMAL CONDUCTIVITY OF MULTIWALL CARBON NANOTUBES BASED NANOLUBRICANTS BY 3 OMEGA METHOD"** completed by **ABDULKAREEM ALASLI** under supervision of **ASSOC. PROF. DR. ALPASLAN TURGUT** and we certify that in our opinion it is fully adequate, in scope and in quality, as a thesis for the degree of Master of Science.

Assoc. Prof. Dr. Alpaslan TURGUT

Supervisor

Assist. Prof. Dr. Ziya Haktan Karadeniz

(Jury Member)

Assoc. Prof. Dr. Levent Çetin

(Jury Member)

Prof. Dr. Kadriye ERTEKİN

Director

Graduate School of Natural and Applied Sciences

ACKNOWLEDGMENT

"*O Allah, any blessing I, or any of Your creation risen upon, is from You alone, without partners. To You goes All the praise and all gratitude."* [Hadith]

My deepest appreciation belongs to my supervisor, Associated Professor Dr. Alpaslan TURGUT for his unlimited support and kindness along my stay in Dokuz Eylül University. I would like to thank him also for his trust to give me such a fascinating subject. His trust and support fulfilled my dream and brought me valuable experiences of working with several extraordinary nano-materials and to be familiar with publishing and conducting research skills. Thank you for believing in me!

I would like also to express my deepest gratitude to my TÜBITAK-project supervisor, Associated Professor Dr. Levent ÇETİN, who provided me the opportunity to join his research team. Without his precious support it would not be possible to conduct this research. I really appreciate you for everything!

I would also like to express my thanks to Assoc. Prof Dr. Ziya Haktan KARADENİZ, to all Dokuz Eylül group members -Serkan DOĞANAY, Tuba EVGİN, Alper Mete GENÇ, Halil Doğacan KOCA and Alim ZORLUOL- and to TEME group members -Nail AKÇURA, Aytaç KAHVECİ, Serpil AŞKIN and Mustafa Volkan YAZAICI- for their nice and warm attitude toward me during the time I spent there. You are like my family, I'll never forget you all!

I would like to thank the jury members and Assis. Prof. Mehmet Akif EZAN for his insightful comments which incented me to widen my research from various perspectives.

Meanwhile, it is my great pleasure to thank the Yurtdışı Türkler ve Akraba Topluluklar Başkanlığı and Turkey scholarship association for this opportunity and for their support during my stay in Turkey. Thank you!

Above all, I would like to send my ultimate love to my family for their permanent support during my whole life, especially my beloved grandfather and grandmother. May almighty Allah give you the best place in his paradise. I REALLY MISS YOU!

Abdulkareem ALASLI

MEASURING THE TEMPERATURE DEPENDENT THERMAL CONDUCTIVITY OF MULTIWALL CARBON NANOTUBES BASED NANOLUBRICANTS BY 3 OMEGA METHOD

ABSTRACT

The main purpose of this study is to utilize the well-known three-omega method for accurately measuring and inspecting the thermal conductivity of multiwall carbon nanotubes nanolubricants under the influence of temperature. For that, pure multiwall carbon nanotubes, without any special treatment, were dispersed in six types of oils at three different weight concentrations (0.05, 0.1 and 0.3 percent by weight) by ultrasonication and without using any stabilization method.

First, the study focused the light for the first time on the recognized re-dispersion ability of the sonicated multiwall carbon nanotubes within oil. After full agglomeration, it was realized that agitating, shaking or even blowing compressed air on the agglomerated nanolubricant is able to break down the aggregation of the tubes. Quantitatively, viscosity, thermal conductivity and particle size distribution measurements were employed to evaluate the re-dispersion quality. It was observed that the sonicated tubes are separated, saturated, lubricated, and surrounded by oil layers, which not only ease its motion within the lubrication oil, but also counter balanced the Van der Waals forces which give them the ability of detaching by applying any slight force. Microscopic video is presented to clarify the behavior of the tubes during the re-dispersion process. Second, Thermal conductivity measurements were then performed with respect to temperature. The high sensitivity of the three-omega lab-made setup allowed to observe that the thermal conductivities of the nanolubricants peak at specific temperatures and then decay to the value of the base oil. Moreover, microscope images revealed that heating the nanolubricants to higher temperatures (60 to 80 degrees Celsius) resulted in agglomeration of the tubes due to the disappearance of the oil separation layers. Moreover, convection currents act as agitator which also increases the contacts between the multiwall carbon nanotubes.

Keywords: Nanolubricant, multiwall carbon nanotubes, Re-dispersion ability, thermal conductivity, viscosity, engine oil

ÇOK KATMANLI KARBON NANOTÜP BAZLI YAĞLAYICILARIN SICAKLIĞA BAĞLI ISIL ILETKENLIĞININ 3 OMEGA YÖNTEMI ILE ÖLÇÜMÜ

ÖZ

Bu çalışmanın temel amacı, üç omega yöntemi ile çift katlı karbon nanotüp içeren nano-yağlayıcıların ısıl iletkenliklerinin sıcaklık etkisi altında, hassas bir şekilde ölçülmesi ve incelenmesidir. Bunun için, bir iyileştirme yapılmamış, saf, çok katmanlı karbon nanotüpler üç farklı kütlesel katkı oranında (yüzde 0,05, 0,1 ve 0,3), altı farklı türdeki yağ ile karıştırılmıştır. Oluşan süspansiyon, herhangi bir stabilizasyon yöntemi uygulanmadan, ses dalgaları ile dağıtılmıştır.

Çalışmanın ilk kısmında, yağ içerisinde dağıtılmış çift katlı karbon nanotüplerin topaklandıktan sonra yeniden dağılma yeteneği üzerine odaklanılmıştır. Taneciklerin tamamen topaklanmasının ardından, tekrar karıştırılması, çalkalaması veya üzerine hava üflenmesi ile birlikte topaklanma ortadan kalkmaktadır. Çok katmanlı karbon nanotüplerin yeniden dağılabilme kalitesinin değerlendirilmesi amacıyla numunelerin viskozite, ısıl iletkenlik ve tanecik boyutu dağılımı ölçümleri yapılmıştır. Bunun sonucunda, taneciklerin birbirinden ayrıldığı, yağlandığı ve yağ tabakası ile çevrelendiği gözlemlenmiştir. Bu da taneciklerin yağ içerisindeki hareketini kolaylaştırmakta ve Van der Waals kuvvetlerini zayıflatmaktadır. Tekrar dağılma işlemi sırasında taneciklerin davranışı mikroskop altında incelenmiş ve ekte video ile sunulmuştur. Daha sonra, sıcaklığa bağlı ısıl iletkenlik ölçümleri gerçekleştirilmiştir. Üç omega yönteminin yükses hassasiyeti sayesinde, sıcaklık artışı ile birlikte, karışımın ısıl iletkenlik değerinin belirli bir değere kadar arttığı, daha sonra yağın iletkenlik değerine kadar düştüğü gözlemlenmiştir. Karışımın yüksek sıcaklık değerlerine (60'dan 80 santigrat dereceye) ısıtılmasının, yağ tabakalarının kaybolmasından dolayı taneciklerin topaklanmasına yol açtığı mikroskop altında görülmüştür. Ayrıca, meydana gelen doğal taşınım etkisi de, taneciklerin birbirine daha fazla temas etmesine yol açarak, topaklanmaya neden olmaktadır.

Anahtar Kelimeler: Nano-yağlayıcı, Çok katmanlı karbon nanotüpler, Yeniden-dağılma kabiliyeti, ısıl iletkenlik, viskozite, motor yağı

CONTENTS

Page

LIST OF FIGURES

Page

LIST OF TABLES

Page

CHAPTER ONE
INTRODUCTION

"There is plenty of room at the bottom" with these famous few words, R. P. Feynman ignited the first spark of the new age revolution of nanotechnology in 1959 (John, 1997). Many years later, exactly in 1993, Masuda, Ebata, Teramae, & Hishinuma (1993) made their contribution to this revolution by dispersing nano-sized solid particles in water. This contribution, named later by Choi et al (1995) as nanofluid, opened a new horizon in the field of nanotechnology. Many intensive researches, consequently, have been being done and their number is growing rapidly as the time goes on, as Figure 1.1 illustrates. The new generation heat transfer nanofluids show notable enhancement in thermal conductivity, and also show a remarkable potential in various engineering applications such as heat exchanging, electronics, automotive and energy industries (Paolucci, Puliti, Paolucii, & Puliti, 2015).

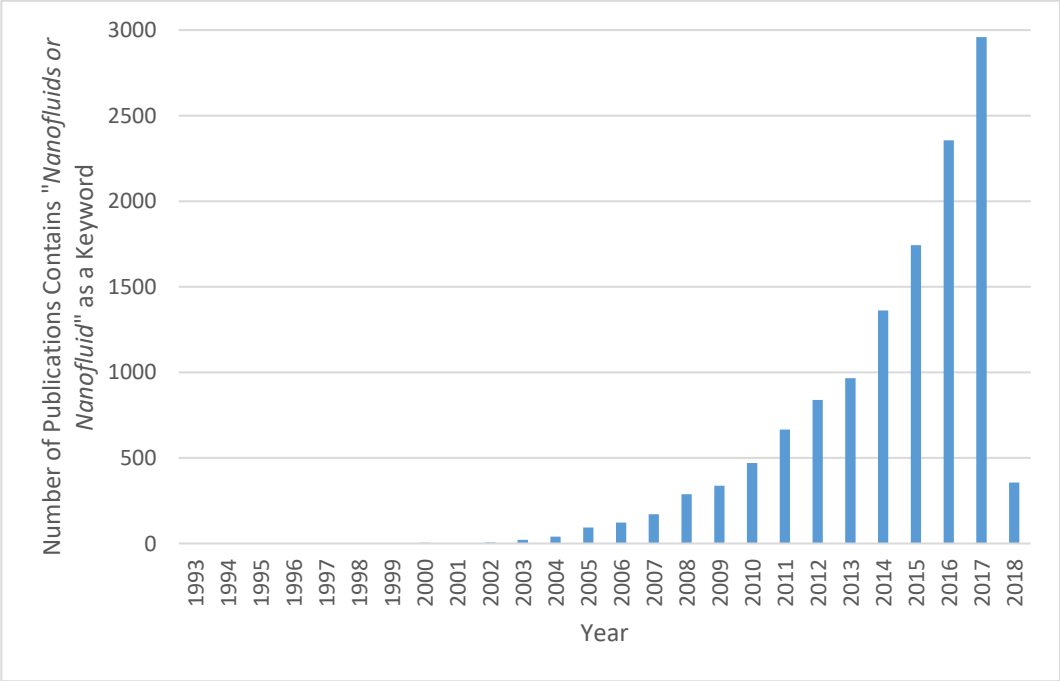

Figure 1.1 Number of publications with respect to the keywords "nanofluids or nanofluids" according to an analysis made with ISI Web of Knowledge (March, 2018)

Nanolubricant, which is another sort of nanofluid, represents nano-sized particles (1-100 nm) suspended within lubrication materials such as mineral oil. Nanolubricant has drawn much attention in the recent years due to the promising achievements in preserving energy consumption, enhancing the surface properties, decreasing the disposal oil, increasing engine efficiencies (Lee et al., 2009) and decreasing the cost of maintenance (Vakili-Nezhaad & Dorany, 2009).

1.1 The Importance and up to Date Investigations of MWCNTs Nanolubricants

Among the various types of nanolubricants, the suspension of carbon nanotubes (CNTs) has unique importance because of their high aspect ratio in addition to their enormous thermal conductivity (3000 W/mK of the multiwall CNTs and 6000 W/mK of the single-wall CNTs (Kim, Shi, Majumdar, & McEuen, 2001)); hence, a great potential for heat transfer enhancement compared to the pure oil (Ding, Alias, Wen, & Williams, 2006).

Choi et al. (2001) achieved the first enhancements in thermal conductivity (2-160%) with the addition of MWCNT at 0.04-1 vol.% to poly α-olefin oil. A subsequence study by Marquis & Chibante (2005), in which they followed the same steps of Choi et al (2001), reported a higher ratio of 175% at the same concentration. Yang, Grulke, Zhang, & Wu (2006), however, reported a surprising 200% enhancement ratio at only 0.34 vol.% by using similar base oil with the addition of Polyisobutene succinimide as surfactant. Shaikh, Lafdi, & Ponnappan (2007) inspected the suspension of the same poly α-olefin oil, but this time, with the addition of functionalized MWCNTS by adding phenyl and carboxylic groups. A high thermal conductivity enhancement up to 160% at 1 vol.% was also obtained. Since these participations, no researcher was able to re-report such high enhancements with different types of oil. Xie, Lee, Youn, & Choi (2003) measured functionalized MWCNTs/decene suspensions with the addition of oleylamine as surfactant, and achieved only 19.6% increase in thermal conductivity at 1 vol %. Several other studies have focused on the suspensions of carbon nanotube within engine oil: Hwang et al. (2007) realized that for the case of CNT with sodium dodecyl sulfate as surfactant, the thermal conductivity of 0.5 vol.% is increased 8.7% compared to the base fluid. Liu et

al. (2005), on the other hand, reported an intermediate thermal conductivity increment, up to 30%, at a 0.02 volume fraction of MWCNT with N-hydroxysuccinimide as dispersant. Ettefaghi, Ahmadi, Rashidi, Nouralishahi, & Mohtasebi (2013) investigated functionalized MWCNT with high viscosity oil for four methods of dispersing at different volume concentrations. The authors suggested that the sample prepared with planetary ball mill at 0.1 wt.% is the most suitable for improving the properties of the engine oil. This sample showed 18% thermal conductivity enhancement with a little reduction in viscosity with respect to the base oil. Three other research groups examined the transformer oil as a base fluid: Beheshti, Shanbedi, & Heris (2014) investigated experimentally the effect of oxidized MWCNTs on the oil thermophysical properties and reported 7.7% thermal conductivity enhancement at 0.01 wt.%; Amiri et al., (2015) used microwave-assisted functionalized MWNTs with hexylamine to increase the enhancement ratio to 10% at 0.005 wt.%; In the work of Fontes et al. Fontes, Ribatski, & Bandarra Filho (2015), higher thermal conductivity enhancement reached, 25.3%. The suspensions were prepared by a high-pressure homogenizer (up to 400 bars). Chen & Xie (2009), however, focused on a different type of oil, silicon oil. A maximum 29% increment was obtained with acid treated MWCNTs and surfactant as an addition. Recently, Ilyas, Pendyala, & Narahari (2017) contributed with an extended study on the thermal oil/MWCNTs nanolubricant without any special treatment or addition, and measured a maximum enhancement of 28.7% with 1 wt.%.

Moreover, among the presented investigations only three have inspected the enhancements of the nanolubricants with the respect of temperature, as can be observed obviously from Table 1.1. The table summarized up to date investigations on MWCNTs/oil in terms of the used based oil, preparation method, concentrations, usage of surfactant, the presented results and the utilized measurement setup for evaluating the thermal conductivity.

Table 1.1 Investigations on suspensions of MWCNTs /different oil-based nanolubricants

Author	Base Oil Type	Concentration	Preparation Method	Surfactant	μ_{nf} Enhancement	k_{nf} Enhancement	Temperature dependence	Measurement setup
(Choi et al., 2001)	poly (α- olefin) oil	0.04-1vol.%	No info	No info	-	2-160%	-	Transient hot-wire
(Y. Yang et al., 2006)	poly (α- olefin) oil	0.04-0.34 vol.%	Ultrasonication	✓	-	6-200%	-	Transient hot-wire
(Shaikh et al., 2007)	poly (α- olefin) oil	0.1-1 vol. %	Ultrasonication& Functionalization	✓	-	33-160%	-	Laser flash apparatus
(Marquis & Chibante, 2005)	poly (α- olefin) oil	0.25-1 vol.%	Ultrasonication	✓	-	1.75	-	Thermal Haake measuring
(Fontes et al., 2015)	Transformer oil	0.005-0.05 vol.%	High pressure homogenizer	-	0.25	0.253	-	Transient hot-wire
(Amiri et al., 2015)	Transformer oil	0.001-0.005 wt.%	Ultrasonication & Functionalization	-	0.09	0.1	30-70 ºC	KD_2 thermal analyzer
(Beheshti et al., 2014)	Transformer oil	0.001-0.01wt.%	Ultrasonication & Functionalization	-	0.009	5.7-7.7%	20-80 ºC	KD_2 thermal analyzer
(Ettefaghi et al., 2013)	Engine oil	0.1-0.5 wt.%	Multi-Methods & Functionalization	✓	Up to 1.7%	13.2-22.7%	-	KD_2-Pro equipment
(M. Liu, Lin, & Wang, 2011)	Engine oil	1-2 vol.%	Ultrasonication	✓	-	8.5-30%	-	Transient hot wire
(Hwang, Park, Lee, & Jung, 2006)	Mineral Oil	0.5 vol%	Ultrasonication	✓	-	0.09	-	Transient hot wire
(Xie et al., 2003)	Decene	0.25-1 vol.%	Ultrasonication	✓	-	4.2-19.6%	-	Transient hot wire
(Ilyas et al., 2017)	Thermal Oil	0.1-1 wt.%	Ultrasonication	-	Up to 66%	Up to 28.7%	25-65 ºC	KD_2-Pro equipment

1.2 Thermal Conductivity Measurement Techniques of Nanofluids and the Chaos in the Reported Results

Over the decades several techniques for measuring the thermal conductivity of fluids have been proposed and a number of them were improved and used for evaluating the nanofluids. Broadly, these techniques can be classified into two categories: *steady state* and *transient techniques*, as summarized in Figure 1.2. The steady state techniques require usually large size specimens and a long period of time to reach thermal equilibrium. After reaching the thermal equilibrium and based on the temperature difference (ΔT) due to the applied amount of heating power, the thermal conductivity of a material can be measured, as explained in Fourier law (Equation 1.1).

$$k = \frac{\dot{Q}.L}{A.\Delta T} \tag{1.1}$$

where, k [w/mK]is the measured thermal conductivity, $\dot{Q}$[W]is the applied amount of power flow through the sample in term of heat, A [m^2] the cross section of the heated sample, ΔT [K] the measured temperature difference, L [m] is distance between the thermal sensors.

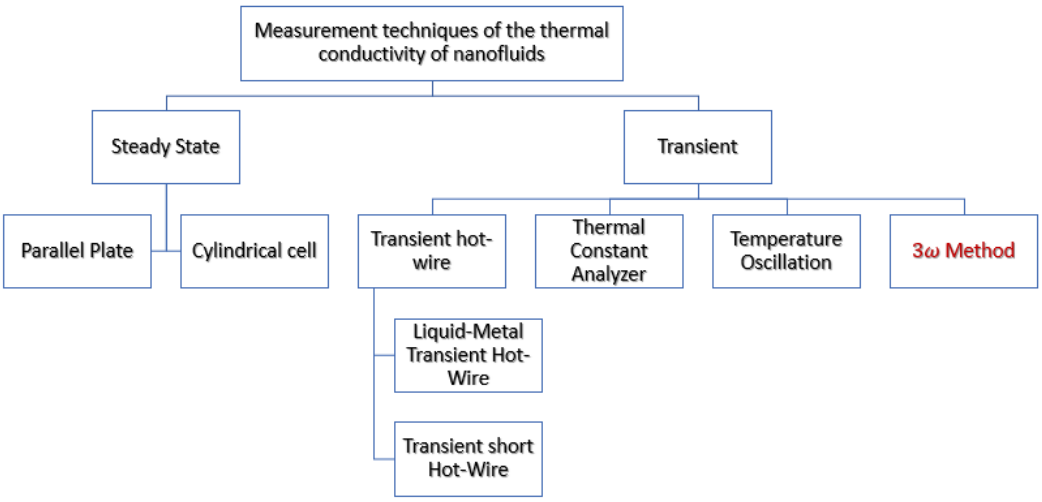

Figure 1.2 Thermal Conductivity measurement techniques for nanofluids

On the other hand, the transient method was developed to overcome the issues of the stead-state method such as error due to heat losses, the long delay of time to reach

thermal equilibrium and the contact thermal resistance of the thermal sensors. The new techniques depend on an embedded plane, strip or wire in the measured specimen which works simultaneously as a heater and thermometer. The embedded part is stimulated by an unsteady current (AC or pulsed) resulting in heat penetrating into the specimen. Consequently, by observing the change in temperature generated by the heat during the measurement. The value of the thermal conductivity of the sample can be determined. As the Figure 1.2 shows, based on the transient method a large group of measurement setups were developed based on the transient method. Moreover, due to their quicker performance and the small required scale of samples, employing these techniques was increasingly favored in the last past years. Out of all the measurement methods, the transient hot-wire method was used much more frequently than the others for evaluating the thermal conductivity enhancement of the nanofluids, as illustrated in Figure 1.3.

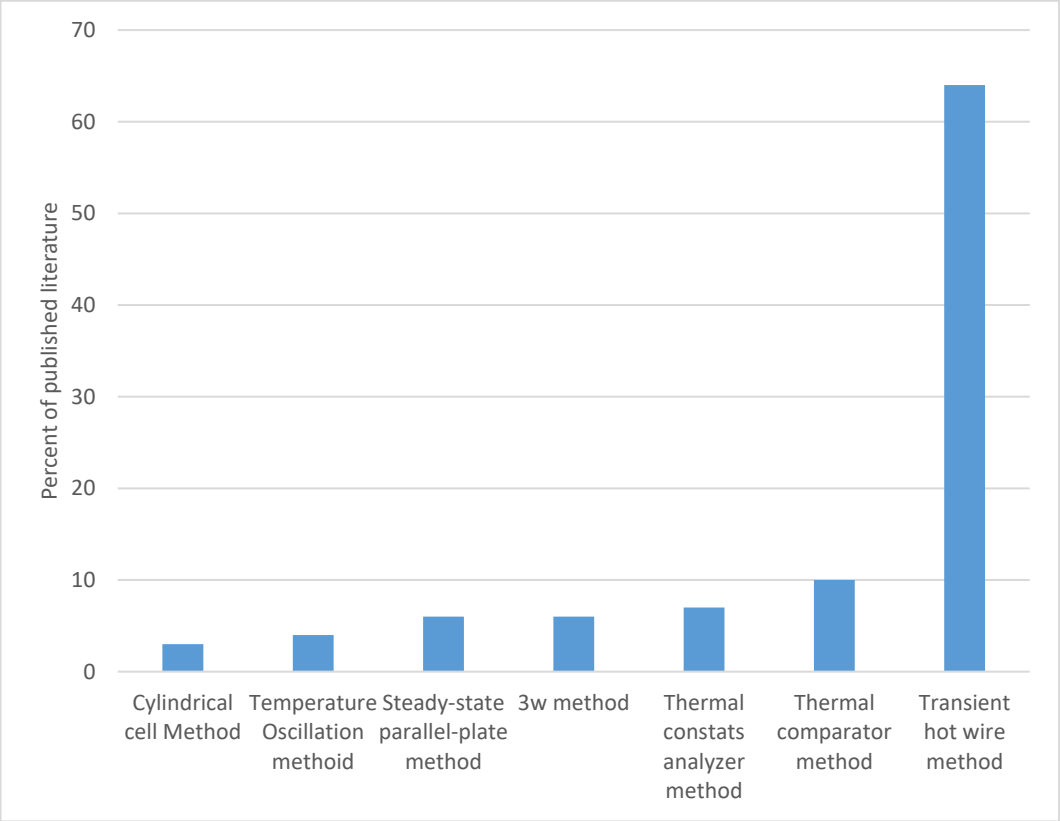

Figure 1.3 The usage rate of the thermal conductivity measurement techniques in the published literature (Paul, Chopkar, Manna, & Das, 2010)

The variety in the used measurement methods, in addition to unsatisfying the necessary conditions for accuracy, resulted in a massive chaos in the reported results. Figure 1.4 demonstrates an example of this chaos by the enhancement of the thermal conductivity of water\MWCNTs. The inconsistency between the results are extreme and 22 of 24 investigations declared that the used instrument is the transient hot-wire technique. The simplifications in the techniques for commercial reasons could led to less accurate results. Thus, the claimed observation of the enormously and unexpected thermal conductivity enhancements of nanofluids may have been attributed to unreliable experimental setups (Antoniadis, Tertsinidou, Assael, & Wakeham, 2016).

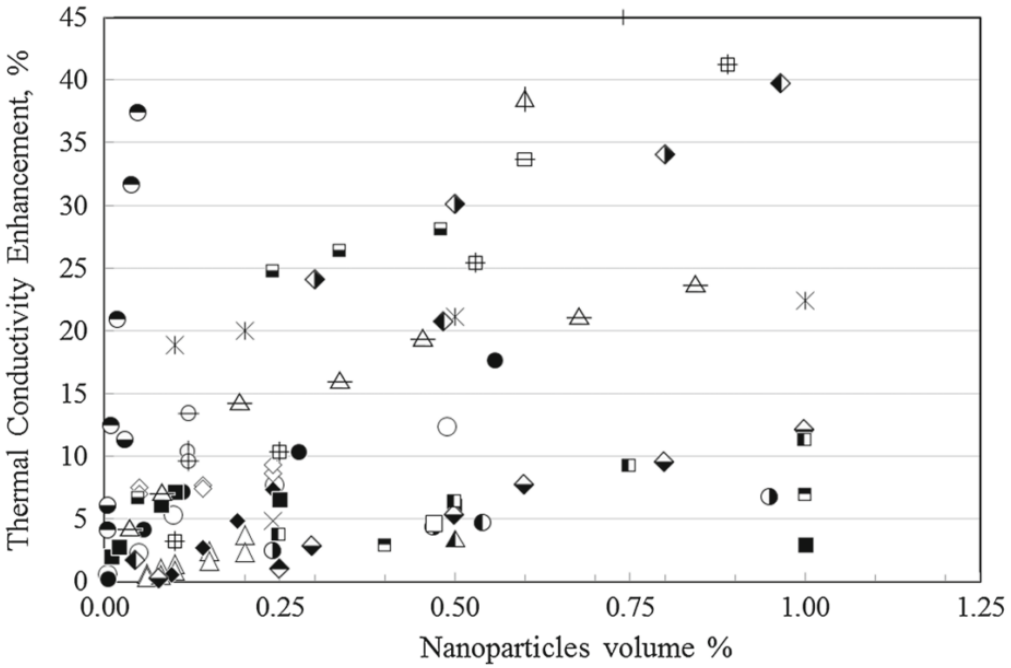

Figure 1.4 The chaos in the provided thermal conductivity enhancement of MWCNT/water based on 24 investigations used hot transient wire (Antoniadis et al., 2016) (Reader is referred to the original paper for the markers labels)

Similarly, Figure 1.5 shows that the obtained enhancements in thermal conductivity of the previously discussed investigations, in which MWCNTs were dispersed within several types of oils, also deviate widely. Furthermore, all of the presented results were measured at the room temperature. This means that at a wider range of temperature the discrepancy in results may go more widely. Therefore, a new trustworthy method to determine the thermal conductivity of nanofluids is of a great need and importance.

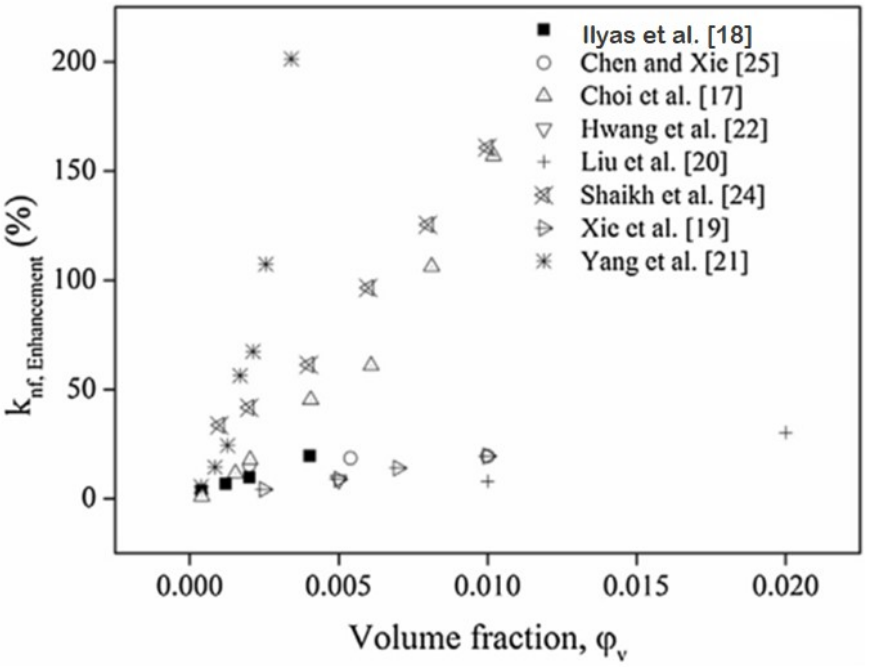

Figure 1.5 Comparative effective thermal conductivity enhancements of MWCNT/Oil nanolubricants

1.3 The 3ω Method

Originally, the 3ω method was first developed by (Corbino, 1911) to determine the thermal diffusivity of metal filaments used in incandescent light bulb. Many years later, (Birge & Nagel, 1987) applied the same method to determine the specific heat and the thermal diffusivity of fluids and dielectric solids. Nevertheless, the 3ω method did not receive much attention until (Cahill & Pohl, 1987) reported its first usage in measuring the "Thermal conductivity of amorphous solids above the plateau", as they titled their paper. Their main aim was to eliminates the thermal conductivity measurement errors which is caused by blackbody radiation. Since Cahill & Pohl (1987) participation, the research area and the number of the investigations which utilized the 3ω method growth exponentially. Most of the research focus mainly on evaluating the thermal characteristics of the thin films (Borca-Tasciuc, Kumar, & Chen, 2001), graphene (Jang et al., 2015), superlattices (C. Dames & Chen, 2004), or any other related planar materials. The 3ω method was also employed in a quite interesting scopes such as gas concertation detection (Kommandur, Mahdavifar, Jin, Hesketh, & Yee, 2016). Moreover, a measurement device based on the 3 ω method was most recently developed to inspect the thermal characteristics of the human skin

(Tian et al., 2017). The applications of 3ω method distributed based on the research area are illustrated in Figure 1.6.

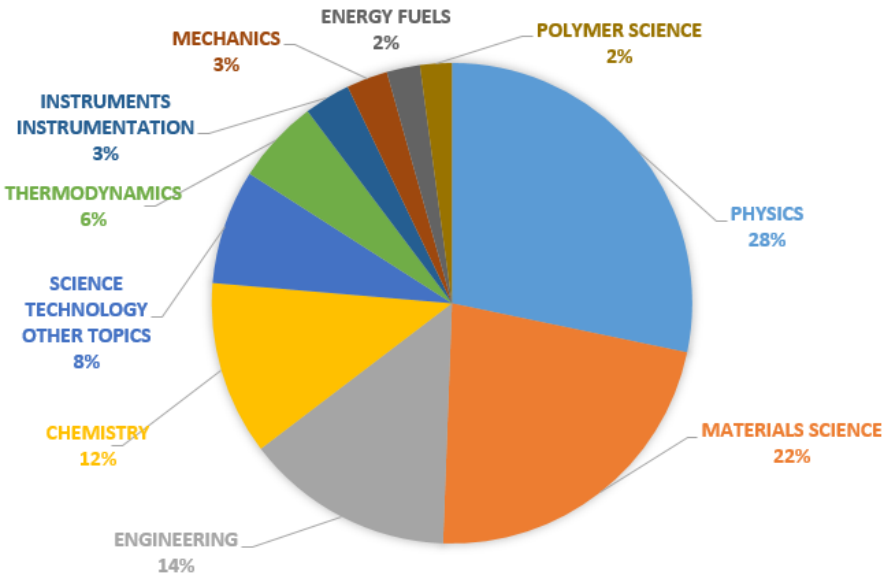

Figure 1.6 The applications of 3ω method distributed base on the research area according to an analysis made by ISI Web of Knowledge

The 3ω method is also developed to estimate the thermal characteristics of fluids and nanofluids. (Yang & Han, 2006) measured the thermal conductivities of liquids from the slope of temperature differences at the 2ω. (Choi, Kim, & Kim, 2007), on the other hand, developed a measurement device which consists of a metallic strip and a dielectric thin film deposited on the surface of a glass substrate. (Turgut et al., 2008) and (Wang, Tang, Liu, Zheng, & Araki, 2007) reported simultaneously the first usage of the 3ω hot wire method on simultaneous thermal conductivity k and diffusivity α measurement of nanofluids. Many works, since then, were initiated by developing experimental setups established on the 3ω. Most of the reviews and the carried-on researches agreed that the measuring devices based on the 3ω methods have proven to be reliable and valuable for measuring the thermal properties of various systems as Chris Dames & Chen (2005) stated.

Nevertheless, to the best of the author's knowledge, most of these investigations have performed their measurements in the room temperature and only few of them

have considered the temperature dependency. Moreover, and to be more specific, the thermal conductivity of MWCNTs/oil nanofluid was investigated only by 3 investigations as Table 1.1 states and none of them utilized the 3ω method in their works

1.4 The Purpose and the Structure of This Thesis

The main purpose of this thesis is to measure the enchantment in thermal conductivity of MWCNTs nanolubricants by using the 3ω method. It also aimed to investigate the influence of temperature and the impact of the interaction between the dispersed nanoparticles on the stability of these obtained enhancements.

This thesis consists of four chapters organized as follows. Chapter 2 discuss the fundamental principle and the theoretical background of the 3ω method. It also explainsin details the utilized measurement setup and its auxiliaries. Chapter 3 outlines the characteristics of the used materials in addition to the followed steps and the used devices to prepare and evaluate the measured samples. Chapter 4 presents and discusses the behavior of MWCNTs inside oil and the effect of this behavior on the thermal conductivity of MWCNTs nanolubricants in the aspect of thermal conduction mechanisms at the nano level. Chapter 4 also presents the enhancements of the viscosity and the thermal conductivity of several MWCNTs nanolubricants and the influence of temperature on them. Finally, Chapter 5 summarizes the findings of this work and suggests relevant potential future works.

CHAPTER TWO
THEORETICAL BACKGROUND

The main purpose of this chapter is to introduce descriptively the main physical theory behind the *3ω* method and related electrical and electronic principles. It also aimed to define the mathematical model with which the thermal conductivity of a material is determined.

Briefly, a totally immersed metal wire within a nanofluid, which is driven by a sinusoidal alternating current (AC) at an angular frequency ω, acts simultaneously as a resistive heater and resistance temperature detector (RTD). The ohmic heating causes a temperature fluctuation at *2ω* depending on the thermal characteristics of the wire and the surrounding material (Chris Dames & Chen, 2005). This disturbs the resistance of the wire also at *2ω* resulting a voltage signal at *3ω* which is much lower (1/1000) than the original signal (AC at 1ω). The thermal conductivity *k* can be determined by detecting the amplitude and the phase of the *3ω* voltage signal and subscribing them in an obtained mathematical model (Cahill, 1990). The *3ω* voltage signal is measured by using a lock-in amplifier with third-harmonic detection. Nevertheless, the large intensity of the *1ω* acts as a noise makes this detection a true challenge. To overcome that, the much larger *1ω* signal should be cancelled either by using Wheatstone bridge (as we have used) or by digital-to-analog converter. Nonetheless, this step can be omitted by employing a developed lock-in amplifier with dynamic reserve (Chris Dames & Chen, 2005). Figure 2.1 illustrates the relationship between the current *I*, the dissipated power *P*, the resistance of the wire *R*, the temperature fluctuation *T* and the voltage V in the 3ω method.

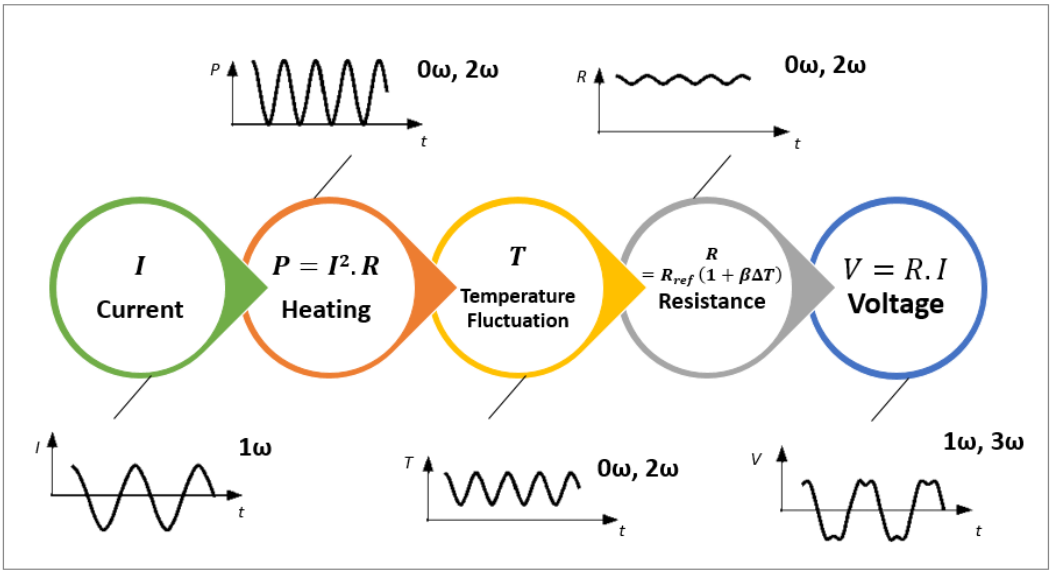

Figure 2.1 Schematic diagram of the relationship between the current *I*, dissipated power *P*, resistance of the wire *R*, temperature fluctuation *T* and the voltage *V* in the *3ω* method

2.1 Mathematical Modulation of the 3ω Method

According to the Joule heating effect, the thermal power dissipated by the wire (resistive heater/RTD) at T_0 due the passing current I can be quantified by the following equation:

$$P = R_0 I^2 \tag{2.1}$$

The alternating current (sinusoidal signal) passing through the wire at frequency ω, however, is given as,

$$I = I_0 cos(\omega t) \tag{2.2}$$

Then, combining Equation 2.2 into Equation 2.1 yields

$$P = R_0 . I_0^2 \cos(\omega t)^2 = \frac{1}{2} R_0 . I_0^2 (1 + \cos(2\omega t)) = \frac{1}{2} R_0 . I_0^2 + \frac{1}{2} R_0 . I_0^2 \cos(2\omega t) \tag{2.3}$$

The dissipating power consists of an oscillating component P_{AC} and constant component P_{DC}, as Equation 2.4 indicates,

$$P = P_{DC} + P_{AC} \tag{2.4}$$

The P_{DC} typically denotes the root mean square (rms) power,

$$P_{DC} = P_{rms} = R_0 I_{rms}^2 = \frac{1}{2} R_0 I_0^2 \tag{2.5}$$

where, $I_{rms} = \frac{1}{\sqrt{2}} . I_0$

Consequently, the temperature of the wire will also rise and oscillate due to the effect of the generated heat (P_{DC} and P_{AC}), as Equation 2.6 shows,

$$T = \Delta T_{DC} + \Delta T_{AC} cos(2\omega t + \phi) \tag{2.6}$$

The ΔT is the increment of the wire temperature with respect to the initial temperature T_0. ΔT_{DC} and ΔT_{AC} are the direct and the oscillating temperature rising components, respectively.

If the surrounding medium of the wire is isolated, the heat stays inside the heater and the temperature oscillation will get higher and higher. On the contrast, if the heat is transferred to the adjacent medium (fluid in our case) at a fix rate, the temperature oscillation will reach an equilibrium state. Based on this, the thermal properties of the surrounding medium can be determined by measuring the resulted equivalent temperature oscillation. Nevertheless, measuring the temperature oscillation directly can be very challenging if not impossible. Hence, another way should be found.

Heating the metal wire perturbs its resistance, as it will be discussed later. Depending on this phenomenon, measuring the temperature oscillation of the wire can be accomplished by measuring the change in its resistance, as it can be realized from Equation 2.7.

$$R(t) = R_0(1 + \beta \Delta T_{DC} + \beta \Delta T_{AC} cos(2\omega t + \phi) \tag{2.7}$$

where β is the temperature coefficient of resistance. β refers to the resistance change factor per degree Celsius of temperature.

Commonly, the resistance can be detected by measuring the resulting voltage across the wire which can be obtained by multiplying the current I by the resistance of the heater R which yields,

$$V(t) = I(t)R(t) \tag{2.8}$$

By substituting 2.7 and 2.2 into 2.8,

$$V(t) = I_0 R_0[(1+\beta\Delta T_{DC})\cos(\omega t) + \frac{1}{2}\beta\Delta T_{AC}\cos(\omega t+\phi) + \frac{1}{2}\beta\Delta T_{AC}\cos(3\omega t+\phi)] \quad (2.9)$$

The resulted voltage consists of three terms as it can be recognized form Equation 2.9. The first term (ΔT_{DC}) is independent of the temperature oscillation. The temperature oscillation ΔT_{AC} of the second term, however, is very small comparing to the first term since β is very small ($\times 10^{-3}$). Thus, it is very difficult to determine its amplitude and phase from the first harmonic (1ω). This leads us to that the amplitude and the phase of the temperature oscillation can only be determined from the component of the 3rd harmonic (3ω), as Equation 2.9 reveals. It is important to mention here that the components of the 1ω is very large (1000 times greater than the 3ω component) and act as a noise that should be eliminated in order to perform clear measurements of the 3ω signal.

Based on that, the voltage of the third harmonic signal (3ω) can be given as,

$$V_{3\omega}(t) = I_0 R_0 \cdot \frac{1}{2}\beta\Delta T_{AC}\cos(3\omega t+\phi) = \frac{1}{2}V_0\beta\Delta T_{AC}\cos(3\omega t+\phi) \quad (2.9)$$

The voltage of the 3ω is composed of a real (*in-phase*) and an imaginary (*out-phase*) components.

$$V_{3\omega} = V_{3\omega\,\text{in phase}} + iV_{3\omega\,\text{out of phase}} \quad (2.10)$$

Accordingly, the components of the temperature can be concluded as,

$$\Delta T_{AC} = \Delta T_{AC\,\text{in phase}} + i\Delta T_{AC\,\text{out of phase}} = \Delta T_{AC}(\cos(\phi) + i\sin(\phi)) \quad (2.11)$$

In the following section, the equation which relates the temperature oscillation with the thermal conductivity of the surrounding medium will be derived. Once again, this equation is used for determining the thermal conductivity of the nanofluid k_f.

2.2 One-dimensional (Line) Heater Inside a Material

Cahill derived in his famous paper (Cahill, 1990) the formula of thermal conductivity depending on the frequency of the temperature oscillation instead of the

time decency at distance x. He started his derivation based on the Equation of the heat conduction of an infinite heat source presented by Carslaw & Jaeger (1959),

$$\frac{1}{\alpha}\frac{\partial T}{\partial t}=\frac{\partial^2 T}{\partial r^2}+\frac{1}{r}\frac{\partial T}{\partial r}+\frac{1}{r^2}\frac{\partial^2 T}{\partial \theta^2}+\frac{\partial^2 T}{\partial z^2} \tag{2.12}$$

where α is the thermal diffusivity $\alpha = k/\rho.c_p$ [m^2/s], k [W/mK], ρ [kg/m^3] and c_p [J/kgK] are the thermal conductivity, the density and the specific heat capacity of the material.

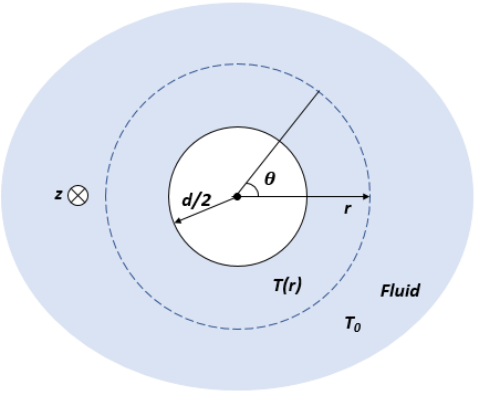

Figure 2.2 Schematic diagram of the wire (linear heater) cross section and the surrounding medium

For simplifying Equation 2.12, it is assumed that the exited wire is one-dimensional heater and thus the only temperature gradient occurs radially (r). Based on that the temperature gradient along z (axial) and θ (circumferential) directions are equal to zero. Mathematically,

$$\frac{1}{\alpha}\frac{\partial T}{\partial t}-\frac{\partial^2 T}{\partial r^2}-\frac{1}{r}\frac{\partial T}{\partial r}=0 \tag{2.13}$$

The temperature of the material adjusting the wire $T(r,t)$ is equal to the sum of the ambient temperature T_0 and the rise in temperature due to both the DC component $\Delta T_{DC}(r)$ and the temperature oscillation $\Delta T_{AC}(r,t)$,

$$T(r,t)=T_0+\Delta T_{AC}(r,t)+\Delta T_{DC}(r) \tag{2.14}$$

As declared previously, the thermal conductivity is related to the temperature oscillation after reaching the steady state. Therefore, the DC component is neglected and Equation 2.14 becomes,

$$\frac{\partial^2}{\partial r^2}[T_{AC}(r,t)] + \frac{1}{r}\frac{\partial}{\partial r}[T_{AC}(r,t)] - \frac{1}{\alpha}\frac{\partial}{\partial t}[T_{AC}(r,t)] = 0 \qquad (2.15)$$

This equation can be solved by the separation of variables,

$$\Phi(r,t) = \Delta T_{AC}(r)\Theta(t) \qquad (2.16)$$

$\Delta T_{AC}(r)$and $\Theta(t)$ are the spatial and temporal evolution of the temperature oscillations. As discussed previously, the temperature is also oscillating at the second harmonics (2ω) as the equation of resistance oscillation reveals (2.7). Thus, the temporal evolution can be given as,

$$\Theta(t) = \cos(2\omega t) = \Re(e^{i2\omega t}) \qquad (2.17)$$

Substituting 2.16 and 2.17 in 2.15 resulting,

$$\cos(2\omega t)\frac{\partial^2}{\partial r^2}[T_{AC}(r)] + \cos(2\omega t)\frac{1}{r}\frac{\partial}{\partial r}[T_{AC}(r)] - \frac{1}{\alpha}T_{AC}(r)\frac{\partial}{\partial t}[\cos(2\omega t)] = 0 \qquad (2.18)$$

$$\cos(2\omega t)\frac{\partial^2}{\partial r^2}[T_{AC}(r)] + \cos(2\omega t)\frac{1}{r}\frac{\partial}{\partial r}[T_{AC}(r)] - \frac{i^2 2\omega}{\alpha}T_{AC}(r)\sin(2\omega t) = 0 \qquad (2.19)$$

$$\Re\left[\left(\frac{\partial^2}{\partial r^2}[T_{AC}(r)] + \frac{1}{r}\frac{\partial}{\partial r}[T_{AC}(r)] - q^2 T_{AC}(r)\right)e^{i^2\omega t}\right] = 0 \qquad (2.20)$$

where $q = \sqrt{i^2\omega/\alpha}$ (rad/m) is the wave number of the thermal wave.

As it can be realized from Equation 2.20, $\frac{\partial^2 T_{AC}(r)}{\partial r^2} + \frac{1}{r}\frac{\partial T_{AC}(r)}{\partial r} - q^2 T_{AC}(r) = 0$, is the Bessel function of order zero and argument qr. The solution of this function is from the shape,

$$y = c_1 I_q(x) + c_2 K_q(x) \qquad (2.21)$$

$I_z(x)$ and $K_z(x)$ are the modified Bessel function of order z and argument x. Consequently, Equation 2.20 becomes,

$$\Delta\Phi(r,t) = \Re\left[c_1 I_0(qr) + c_2 K_0(qr)\right)e^{i^2\omega t}] \qquad (2.22)$$

Constants C_1 and C_2 can be determined by applying the boundary conditions. First, when the diameter of the wire increases to infinity, the temperature oscillation decays to zero. In other words, $I_q(x)$ goes to infinity and $K_q(x)$ approach zero.

$$I_0(q\infty) \to \infty \tag{2.23}$$

$$K_0(q\infty) \to 0 \tag{2.24}$$

$$\Delta T(\infty, t) \to 0 \tag{2.25}$$

Substituting the boundary conditions in Equation 2.22, the value of first constant becomes zero $\boldsymbol{c_1=0}$

Second, when the diameter of the wire tends to zero, the rate of the oscillating heat conduction is given by,

$$\dot{Q_w} = \Re\left[P_{rms}e^{i2\omega t}\right] = \lim_{r\to 0}\left[-kA_s\frac{\partial\Phi(r,t)}{\partial r}\right]_{r=\frac{d}{2}} \tag{2.26}$$

where $A_s=2\pi rl$ [m^2] is the cross-section area of the wire, k is the thermal conductivity of the material and $\dot{Q}_w$ [W] is calculated according to Fourier's law of one dimensional heat conduction $\dot{Q_w} = -kA_s\frac{\partial T}{\partial r}$.

$$\dot{Q_w} = \Re\left[P_{rms}e^{i2\omega t}\right] = \lim_{r\to 0}\left[-kA_s\frac{\partial}{\partial r}\left(c_2K_0(qr)\right)e^{i2\omega t}\right]_{r=\frac{d}{2}} \tag{2.27}$$

For small values of $qr<<1$ the value of the modified Bessel function becomes $K_0(qr)=-ln(qr)$ then,

$$C_2 = \frac{p_{rms}}{2\pi k}, \tag{2.28}$$

where $p_{rms} = \frac{P_{rms}}{l}$

Substituting the value of C_1 and C_2 in Equation 2.22 yields,

$$\Delta\Phi(r,t) = \Re\left[\frac{p_{rms}}{2\pi k}K_0(qr)e^{i2wt}\right] = \left|\Delta T_{AC}\right|\cos(2\omega t+\phi) \tag{2.29}$$

Comparing with Equation 2.11

$$\Delta T_{AC}(r,2\omega) = \frac{p_{rms}}{2\pi k}K_0(qr) = \Delta T_{AC\text{ in phase}} + i\Delta T_{AC\text{ out of phase}} \tag{2.30}$$

where,

$$\Delta T_{AC\,\text{in phase}} = \frac{p_{rms}}{2\pi k}\Re[K_0(qr)] \tag{2.31}$$

$$\Delta T_{AC\,\text{out of phase}} = \frac{p_{rms}}{2\pi k}\Im[\frac{p_{rms}}{2\pi k}K_0(qr)] \tag{2.32}$$

To conclude in few words, the solution of temperature oscillation is extracted starting from the equations of the heat conduction of an infinite linear heat source. The resulting Equations 2.30 and 2.31 express that the temperature oscillation is induced as an interaction of the linear heater immersed within fluid and has the form of modified Bessel function of the zero order and the second kind.

The temperature oscillation decays quickly due to the effect of modified Bessel function ($K_0(qr)$), as shown in Figure 2.3. Nevertheless, it shall be assured that the oscillation is contained within the fluid. Otherwise, the thermal conductivity of the container will be measured. This can be done be finding the thermal wave penetration depth λ, as illustrated in Equation 2.32. To consider a specimen as a semi-infinite medium, its thickness should exceeds 5 times the thermal penetration depths (Cahill, 1990).

$$\lambda = \frac{1}{|q|} = \sqrt{\frac{\alpha}{2\omega}} \tag{2.31}$$

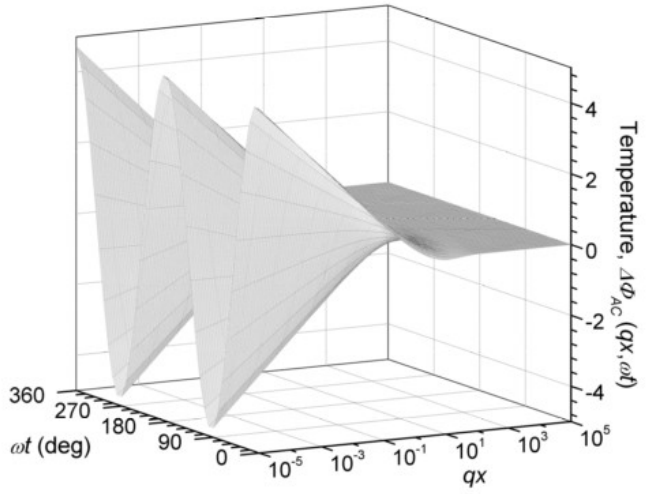

Figure 2.3 The real part of Equation 2.28. The oscillations decay rapidly as it goes far from the heater

2.3 Model Based on the Interface Heat Impedance

In the previous section, temperature oscillation for a line heater immersed inside an infinite cylinder was derived. The thermal conductivity can be determined based on the slope of the real (in-phase) components of the thermal oscillations versus the temperature excitation at 2ω (frequency dependence). However, Turgut et al. (Turgut et al., 2008) developed a different model based on the work of (Chirtoc & Henry, 2008a) for micro-heat transfer measurements used in scanning thermal microscopy (SThM), which is presented as follow.

Starting from defining dimensionless impedance F as (Chirtoc & Henry, 2008b) derived,

$$F = \frac{Z_s}{Z_p} = \frac{z_s / 2\pi r l}{l / \pi r^2 k_p} = \frac{k_p r}{2l^2} z_s \tag{2.33}$$

where z_s is the specific thermal impedance at the interface $z_s = \frac{Z_s}{2\pi r l}$, Z_p is the thermal resistance of the wire in the axial direction for an ideal infinite long thin wire.

The thermal impedance Z_s is given as,

$$Z_s = \frac{\theta_{2\omega}}{P_{2\omega}} \tag{2.34}$$

The temperature oscillation according to Equation 2.28,

$$\theta(r,2\omega) = \frac{P_{2\omega}/l}{2\pi k_s} K_0(qr) \tag{2.35}$$

As mentioned previously, at low frequency (q<<1) the modified Bessel function becomes $K_0(qr) = -\ln(qr)$ and Equation 2.32 can be approximated as (Cahill, 1990),

$$\theta_{2\omega} = \frac{P_{2\omega}}{2\pi k_s l^2}\left[\ln\frac{\mu_s}{1.2594 r} - i\frac{\pi}{4}\right] \tag{2.36}$$

where, μ_s=1/q. By substituting 2.36 and 2.34 in Equation 2.32, it becomes,

$$F = \frac{k_p r^2}{2k_s l^2}\left[\ln\frac{\mu_s}{1.2594 r} - i\frac{\pi}{4}\right] \tag{2.37}$$

where, k_p an k_s are the thermal conductivity of the metal wire and the sample, respectively.

2.4 Model for Measuring the Thermal Conductivity of a Nanofluid Relatively on its Based Fluid

Most of the works, related to the 3ω method, construct the model from which the thermal conductivity is determined based on the real part of Equation 2.29. However, Turgut et al. (Turgut et al., 2008) measured the thermal conductivity of the nanofluid relatively to the one of the base fluid by taking the ratio of the imaginary parts of Equation 2.36 for the measured nanofluid over the imaginary part for its base fluid at a specified frequency, as stated in Equation 2.37. This is because, unlike the other measurement setups, the used thermal probe (ThP) is independent of the sample (detachable) which allows several measurements for different samples with a single ThP probe.

$$\frac{k_s}{k_b} = \frac{\Im[F_b]}{\Im[F_s]} \tag{2.38}$$

Where, k_s and k_b are the thermal conductivity of the sample and the base fluid, respectively. Moreover, Turgut et al. stated based on his research that there is an optimum frequency range (0.5 Hz $\leq f \leq$ 2 Hz) at which this model yields to stable results with negligible error, as Figure 2.4 reveals.

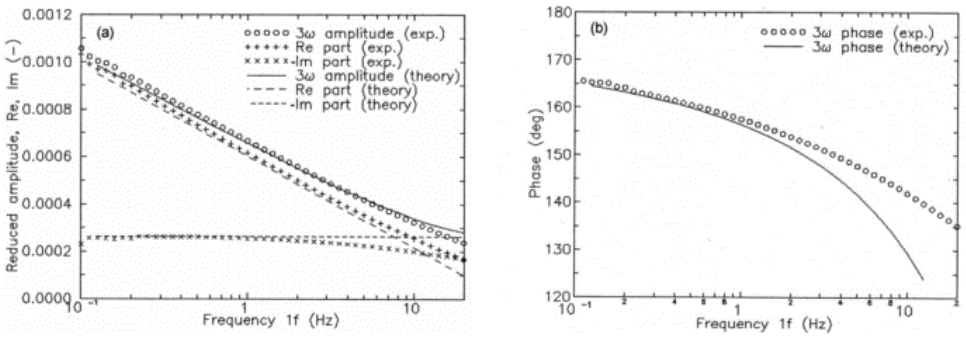

Figure 2.4 The agreement between theoretical and experimental results for water ((a) for amplitude and (b) for phase, according to Equation 2.36) (Turgut et al., 2008)

2.5 The Effect of Changing the Sample Temperature

The length of the wire (L) and its diameter (d) define the resistances and thus the voltages that can be measured when a current is flowing across it. This can also be stated by Ohm's law for a uniform conductor,

$$R = \rho \frac{L}{A} \tag{2.39}$$

Where, R [Ω], L [m], A [m^2] are the resistance, the length and the cross-section area of the wire, respectively. ρ [Ω.m] is the static resistivity of the wire material.

As in any conductive material, the electrical resistivity of the wire is a temperature dependent parameter, which means their resistance vary with the changes in temperature. Based on this phenomenon, resistance temperature detectors are fabricated (RTD) for accurate and consistent temperature measuring sensors or heat dissipation indicators, as in our case. Equation 2.38 is used to determine the resistance of a conductor R at any temperature T other than the reference temperature (T_{ref}, generally 20 ºC) at which the standard resistance (R_0) is determined.

$$R = R_0(1 + \beta(T - T_{ref})) \tag{2.40}$$

Where, β is the temperature coefficient of resistance. β refers to the resistance change factor per degree Celsius of temperature. The material of the wire should be selected with adequately high β in order to increase the sensitivity of the wire with the change in temperature. β can take either positive or negative values. The positive values indicate that the resistance of the conductor (typically pure metals) increases with the increment of temperature. On the other hands, the negative values indicate the opposite such in the case of semiconductor materials.

The wire acts as a thermal probe or RTD, as mentioned previously. The relationship between the resistance of RTD and the ambient temperature is highly related. Thus, it worth mention here that since the 3ω measurement setup will be utilized to measure the thermal conductivity of nanolubricants at several higher temperatures, the effect of this phenomenon on the signal of 3ω should be considered in the mathematical model and the cancellation of the 1ω as it will be explained in the following section.

2.6 The Effect of Changing the Surrounding Medium Temperature on the Voltage of the 3ω Signal

To the best of the author's knowledge, all of the works, which focused on the *3ω* method, considered the room temperature as their reference temperature (T_{ref}=20 ºC). Nevertheless, for measuring the thermal conductivity at higher or lower temperatures, the effect of changing the medium temperature on the induced signal across the wire should be considered.

As Equation 2.8 reveals, the resulted voltage, as discussed previously, consists of three components; two depend on the first harmonic *1ω* and one depends on the third harmonic *3ω*. The *3ω* and one of the *1ω* voltage components are related to the sinusoidal temperature oscillation ΔT_{AC}. The other *1ω* voltage component (the first part of the equation), on the other hand, depends on the direct temperature rising ΔT_{DC}. This means changing the amplitudes of ΔT_{AC} and ΔT_{DC} will change the amplitudes of both $V_{1\omega}$ and $V_{3\omega}$, Simultaneously. In other words, the $V_{1\omega}$ and $V_{3\omega}$ are related with each other (like two linked strings) through ΔT. Thus, any disturbance occurs in one of them will also disturb the other.

$$V(t) = I_0 R_0[(1+\beta\Delta T_{DC})\cos(\omega t) + \frac{1}{2}\beta\Delta T_{AC}\cos(\omega t+\phi) + \frac{1}{2}\beta\Delta T_{AC}\cos(3\omega t+\phi)] \quad (2.41)$$

Now changing the temperature of the sample T_s simultaneously affects and changes three essential parameters:

- The thermal conductivity of the measured material itself k_s since it is a temperature dependent parameter. As a consequence, it will change the amplitude of the temperature oscillation ΔT_{AC} since it also related to k_s.

- The resistance of the wire R due to the change in value of the direct ΔT_{DC} and the amplitude of the oscillated temperature rises ΔT_{AC}, as Equation 2.42 reveals,

$$R(t) = R_0(1 + \beta\Delta T_{DC} + \beta\Delta T_{AC}cos(2\omega t + \phi) \quad (2.42)$$

- The voltage across the wire V with its three previously discussed components ($V_{1\omega}$ and $V_{3\omega}$) as a result of changing the two previous parameters (R and ΔT_{AC}).

The model (Equation 2.38) based on which the thermal conductivity of the material is determined is not affected by changing the temperature of the material since it is already considered in the thermal conductivity of the material k_s and the argument of the modified Bessel function $K_0(qr)$. Nevertheless, the amplitude of the first harmonic 1ω signal, which acts as a noise that should be eliminated in order to perform clear measurements of the 3ω signal, changes notably. Therefore, the effect of changing sample temperature should be considered in the electronic device that is responsible of cancelling the noise of the 1ω, as it will be declared in the next chapter. Moreover, changing the temperature will disturb 3ω signal and the system for a period of time (transient region) after which the system reaches equilibrium (steady state) again, as Figure 2.5 indicates. This phenomenon should also be considered while measuring the thermal conductivity with continuously changing the temperature.

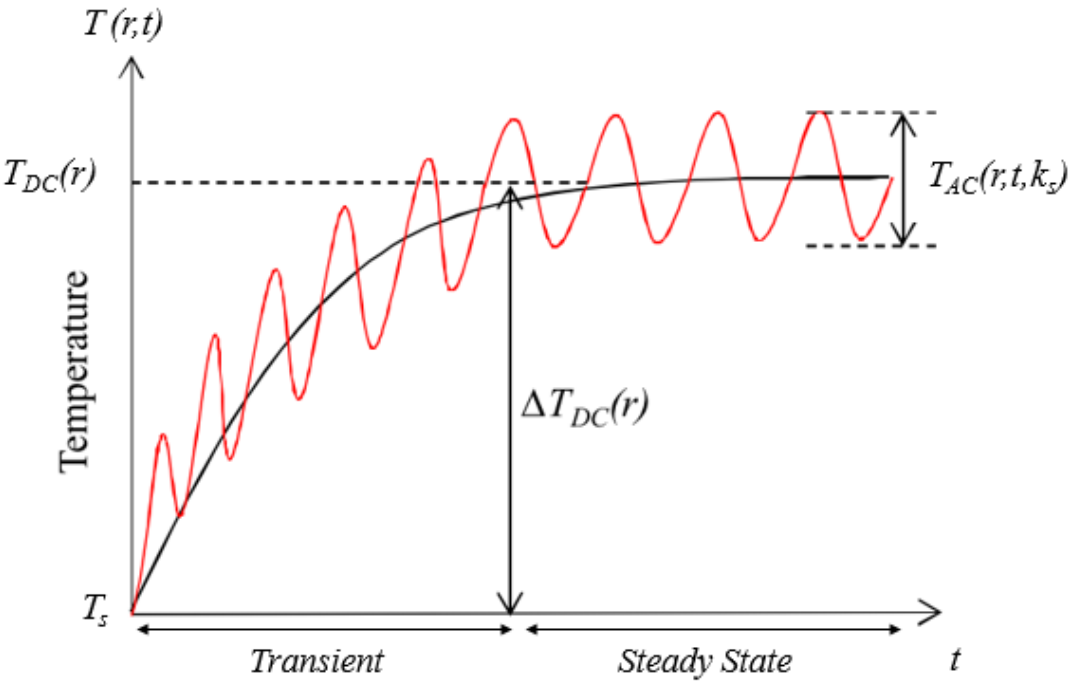

Figure 2.5 Behavior of wire temperature in the transient and steady states

CHAPTER THREE
EXPERIMENTAL SETUP AND SAMPLES PREPERATION

The objective of this chapter is to introduce the utilized 3ω experimental setup with all its components and the characteristics of the used materials. This chapter also contains a description of the preparation and evaluation methods with all auxiliary devices that were employed for inspecting the stability and the viscosity of the studied nanolubricants with their uncertainties.

3.1 Measurements and Uncertainties

3.1.1 Thermal Conductivity Measurement Setup

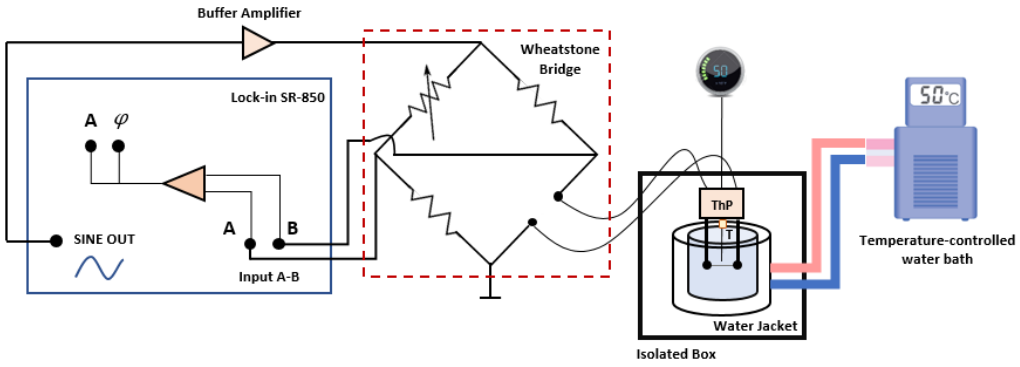

Figure 3.1 Schematic diagram of the 3ω experimental setup consists of (Thermal probe (ThP), Wheatstone bridge, lock-in amplifier, buffer amplifier and hot water bath

A lab-made setup based on the previously explained 3ω method with a hot-wire thermal probe exited by an AC current and a 3ω lock-in detection technique was used to measure the thermal conductivity of the MWCNTs nanolubricants. A schematic diagram of the used setup is shown in Figure 3.1. Briefly, the experimental setup consists of thermal probe (ThP), made of a metallic wire (Nickel) of length $2l$=19.0 mm and diameter $d=50\ \mu m$. The thermal probe is totally immersed in the fluid sample, and acting (as mentioned previously) simultaneously as a heater and as a thermometer. A Sine out current (AC) is applied on the wire at a frequency $f/2$. To achieve a good signal-to-noise ratio, the first harmonic 1ω must be cancelled by a Wheatstone bridge

arrangement (Figure 3.1). The selection of the 3rd harmonic (3ω) form the differential signal across the bridge is performed by a Stanford SR-850 lock-in amplifier tuned to this frequency. The following subsections contain a full description of each of these parts function.

3.1.1.1 Lock-in Amplifier

Stanford Research Systems SR850 is a digital lock-in amplifier based on digital signal processing (DSP). It is typically used to measure the amplitude and the phase of insignificant current or current signals accurately. The SR850 lock-in amplifier is unique with a number of significant features and performance advantages comparing to traditional lock-in amplifiers such as higher digital precision and flexibility, lower deviation, lower distortion, and dramatically higher phase resolution. The amplitude and the phase of 3ω voltage signal was measured by operating the SR850 lock-in amplifier by using a technique called phase-sensitive detection. This technique is used to measure very weak signals in the presence of large amount of noise. In this case, the noise is the exciting current itself (the first harmonic 1ω), whose intensity is roughly 1000 times greater than of the 3rd harmonic signal. Wheatstone bridge is used, however, for cancelling this noise in order to get clearer measurements.

Figure 3.2 Stanford SR-850 lock-in amplifier (Stanford, 2017)

3.1.1.2 Wheatstone Bridge and the Buffer Amplifier

The second essential part in this experimental measurement setup is the combination of Wheatstone bridge and the buffer amplifier. The excited current at a

frequency *f* is provided from the internal sine signal generator (sine output) in the lock-in amplifier. The intensity (current and voltage) of the output signal, however, is very weak and need to be amplified to induce effectively the temperature field in the wire and here comes the role of the buffer amplifier with the help of an external power source.

The main function of Wheatstone bridge, as mentioned previously, is to eliminate the 1st harmonic (1ω) in order to perform the 3ω measurements more precisely. Simply, the Wheatstone bridge, as illustrated in Figure 3.1, is two series arrangements of resistances linked parallelly and connected to a voltage source. When the two parallel branches are balanced, the output voltage is equal to zero. In our case, the thermal probe (ThP) is one of this resistance and on the other branch is an adjustable resistance. By adjusting the adjustable resistance, the output voltage and hence the 1ω can be cancelled without affecting the 3ω, according to Equation 2.9. This operation is done manually by the help of an oscilloscope (RIGOL DS1102C).

3.1.1.3 Thermal Probe (ThP)

The third essential part is the thermal probe (ThP). The ThP was constructed from a long thin Nickel wire with diameter of 40 μm in and length of $2l$ =19.0 mm fixed on a printed circuit board (PCM), as shown in Figure 3.3. Table 3.1 presents the properties of the used wire.

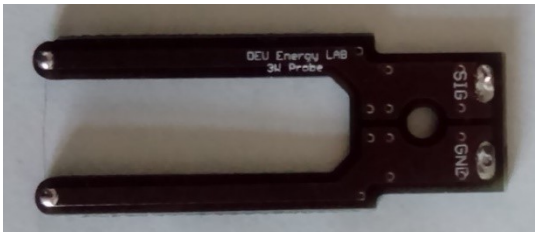

Figure 3.3 The thermal probe ThP (Personal archive, 2017)

The wire is connected directly to both an amplified sinusoidal source signal and the input of a lock-in amplifier at the same time. The signal source ($\pm I$) will generate heat in the wire and the lock-in amplifier will measure the electrical potential ($\pm V$) of the 3rd harmonic signal (3ω) across the wire (heater/thermal probe) simultaneously, as

Figure 3.4 indicates. In other words, the wire works as an input (thermal probe) and output (resistive heater) simultaneously.

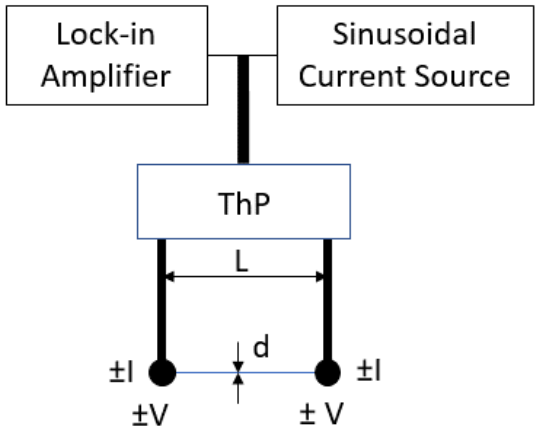

Figure 3.4 Schematic diagram of the wire and its connections

Table 3.1 Characteristics of the used Thermal probe

Characteristics of the Nickel wire (Provided by the producer (Goodfellow, UK))	
Density ρ_p [kg/m^3]	8900
Heat capacity c_p [j/kgK]	444
Thermal conductivity k_p [W/mK]	90.9
Surface Area ρ_{el} [Ω.m]	6.91×10^{-8}
Temperature coefficient of resistance β [1/K]	5.19×10^{-3}

3.1.2 Changing and Fixing Temperature During Measurements

Since the thermal conductivity and the viscosity of the nanolubricants are highly dependent on temperature, it is very important to ensure that the temperature of the sample can be flexibly changed and then fixed at a constant value during and according to the performed measurement. To ensure that, a water jacket in conjunction with the temperature-controlled bath (Polyscience M9712, USA) with a stability of 0.1 °C were operated. In addition, an integrated temperature sensor within the viscometer is also

employed in order to accurately determine and stabilize the samples' temperatures in a short period of time, as shown in Figure 3.5.

Figure 3.5 Temperature-controlled bath (Polyscience M9712, USA)

3.1.3 Effective Viscosity Measurement Setup

A sine-wave Vibro Viscometer SV-10 (A&D, Japan) with a measurement range of 0.3 mPa.s to 10,000 mPa.s, was utilized to measure the effective viscosity of the nanolubricant (Turgut et al., 2009), Figure 3.6. According to the manufacturer, the SV-10 viscometer has two thin sensor plates that are driven with electromagnetic force at the same frequency by vibrating at constant sine-wave vibration in reverse phase like a tuning-fork. The electromagnetic drive controls the vibration of the sensor plates to maintain constant amplitude. The driving electric current, which is an exciting force, will be detected as the magnitude of viscidity produced between the sensor plates and the sample fluid. The coefficient of viscosity is obtained by the correlation between the driving electric current and the magnitude of viscidity.

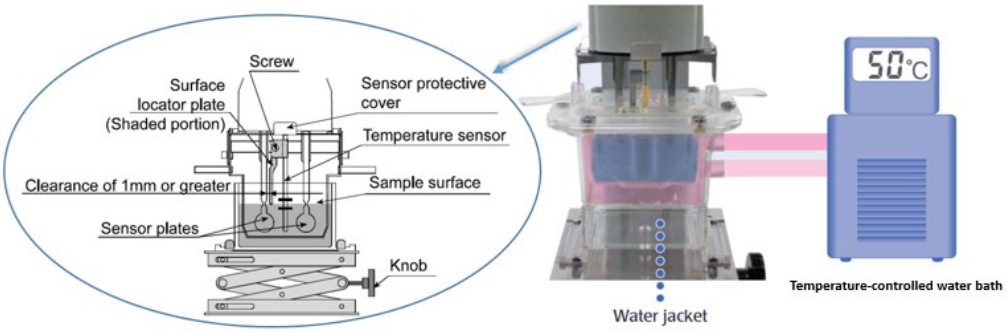

Figure 3.6 Schematic diagram of the viscosity measurement setup (SV-10 Vibro-viscometer with water jacket and temperature-controlled bath)

3.1.4 Evaluating the Stability and Dispersion Quality of the Nanolubricants

Several approaches are proposed in the available literature for evaluating the dispersion quality of a produced nanofluid. For the purpose of this study, particle size distribution (PSD), microscope photographs, with viscosity and thermal conductivity comparison were selected for evaluation. The particle size distribution, which is a common method in several works (Amiri et al., 2015; Ilyas et al., 2017), will present the size range of the deagglomerated MWCNTs directly after ultrasonication and after re-dispersion. This parameter is a good indicator for estimating the quality of the re-dispersion process due to the special behavior of the MWCNTs within oil, as it will be discussed later. The particle size distribution (PSD) of the suspension was analyzed by laser particle size analyzer (Zetasizer Nano-ZS, Malvern Instrument Inc, London, UK), as shown in Figure 3.7. For that, two identical samples were prepared at 0.01 w/v % (according to the instruction of the measurement device).

Moreover, microscope images are also presented to further clarify the behavior of the tubes during heating and the re-dispersion process. This method was also used by Yang et al. (Y. Yang et al., 2006) and Wang et al (J. J. Wang, Zheng, Gao, & Chen, 2012). Inspecting the thermal conductivity and the viscosity of the compared samples are also another way for validation, as an engineering approach. However, it is highly recommended to utilize accurate measurement setups since the characteristics of the nanofluids are very sensitive to any occurred agglomeration of the nanoparticles.

Figure 3.7 Zeta potential and laser particle size analyzer (Zetasizer Nano-ZS) for estimating the particle size distribution with sample holder (DTS1070) (Malvern, 2017)

3.1.5 Uncertainty Estimation

To analyze the uncertainty of the obtained results, all measurements were repeated at least for five times for each concentration. Moreover, all setups were first tested with distillated water and pure mineral oil, then nanolubricants samples were deployed for measurements. A high precision microbalance (Precisa XB 220A), as shown in Figure 3.8, with an accuracy of ±0.1 mg was used to weigh the MWCNTs and the pristine oils samples separately before mixing. The accuracy of the viscometer was verified by comparing the obtained values of the calibration fluid at the considered temperature range (20-60 °C) with the ones provided by the manufacturer. Maximum deviation of 4% was found. Additionally, the accuracy of the temperature measurements, done by the integrated thermometer, is ±0.01 °C. The used 3ω method thermal conductivity measurement setup was validated with measurements made on pure fluids (ethylene glycol and mineral oil) compared to distillated water (k_{sample}/k_{water}), giving k-ratios within the accuracy of ±0.5%. Nonetheless, for the case of repeated measurements, repeatability was found to be within 0.3% to 0.7% at the considered weight concentration range (0.05-0.3 wt.%). In addition to that, Hoffmann

et al. (Hoffmann et al., 2016) also reported close accuracy with similar utilized setup to investigate the temperature dependence of thermal conductivity of vegetable oils.

Figure 3.8 High precision microbalance (Precisa XB 220A) used to weigh the MWCNTs and the pristine oils (Precisa, 2016)

3.2 Materials

Widely used commercial materials were used for synthesizing the nanolubricant samples in order to achieve more realistic results. The first chosen mineral oil was drained from a commercial compressor, which is used in manufacturing home refrigerators (HXK12AA, R600a as a refrigerant, ACC, China). The other oils were brought from well-known engine oil producer. It worth mentioning here that the chosen base oils were selected to cover a wide range of viscosity, as Table 3.1 indicates.

Table 3.2 Characteristics of the used mineral oils

Oil Type	Mineral Oil (used in refrigerators)	Starpet Curdro	Opet Fulllife	Mobil DTE 20	Sunflower oil	Shell Helix
Density at 25ºC [kg/m^3]	817.8	885	890	876	905	888
Thermal conductivity at	0.122	0.130	0.131	0.123	0.159	0.135
Viscosity at 20ºC [mPa.s]	6.55	186	169.5	44.5	33.7	157.0
Viscosity at 60ºC [mPa.s]	2.02	19,5	18.4	6.7	7.78	19

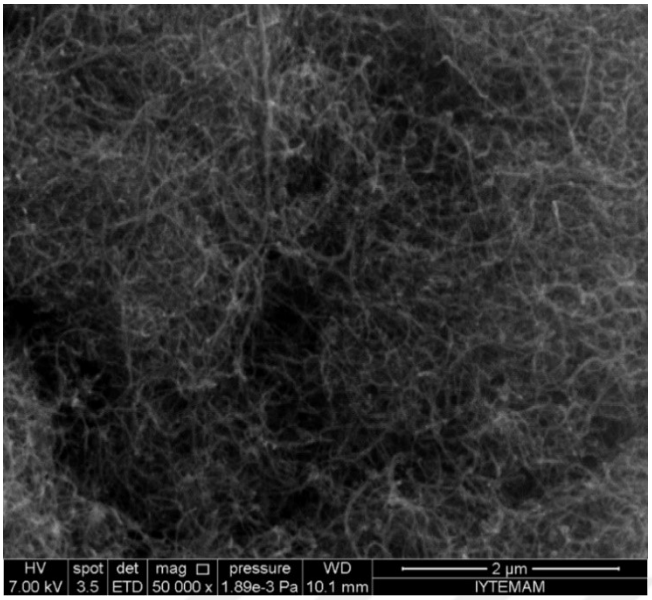

Figure 3.9 Scanning electron microscope (SEM) image of the KNT-M12 MWCNTs (Evgin et al., 2016)

MWCNTs with purity higher than 95% synthesized by (Grafen Chemical Industries Co, Turkey) were used as additive. The No: KNT-M12 was chosen due to its high aspect ratio (small diameter (d= 10 - 20 nm) with long tubes (L=10 – 30 µm)), which plays a great role in increasing the thermal conductivity of the nanofluid (J. J. Wang et al., 2012). Figure 3.1 presents the scanning electron microscope (Philips XL 30S FEG) image that indicates the quality and the dimensions of the chosen MWCNTs; Table 3.1 also summarizes the characteristics of the used MWCNTs. It is important to emphasize here that no surfactant was used since we are trying to observe only the behavior of untreated MWCNTs within pure oil. In addition, surfactants generally participate in reducing the thermal conductivity of the nanolubricant.

Table 3.3 Characteristics of the pristine MWCNTs

MWCNTs (Provided by the producer, (Grafen Chemical Industries Co, Turkey))	
Purity [wt.%]	>95
Average diameter [nm]	10 - 20
Length [µm]	10 - 30
Surface Area [m^2/g]	> 200
Density [kg/m^3]	1911.3 (Evgin et al., 2016)

3.2.1 Nanolubricants Preparation

Stable nanolubricant were obtained by applying the widely used two-steps method (Amiri et al., 2015; Ettefaghi et al., 2013; Hwang et al., 2006; Ilyas et al., 2017; Shaikh et al., 2007; Xie et al., 2003; Y. Yang et al., 2006), as shown if Figure 3.10. The investigated samples were prepared by dispersing precisely measured amounts of MWCNTs within low viscous mineral oil at particle weight concentrations of 0.05, 0.1, 0.2 and 0.3% (i.e. volume concentrations (Eq. 1) of 0.021, 0.043 and 0.128%, respectively). Increasing the concentration over 0.3 wt.%, however, yields to a very viscous nanolubricant (semi-gel) which impedes the experiments. An ultrasonic liquid probe-type processor (Sonicator 3000, MISONIX Co, USA), as shown in Figure 3.11, was employed to break-down the agglomerated MWCNTs in 10 ml mineral oil at a frequency of 20 kHz. Ultrasonication power of 12 W was selected according to the recommendation of the manufacturer for the given volume. A relatively short period of ultrasonication time (40 min) was found to be enough to get homogenous samples as also reported by Ilyas et al. (Ilyas et al., 2017). According to Hilding et al (Hilding, Grulke, George Zhang, & Lockwood, 2007), serious disadvantages occur with over-ultrasonication such as irreversible bends, damage in the wall, breaking the tubes into smaller pieces, and reduce their aspect ratio. Therefore, we tried to minimize the ultrasonication time until the point a homogenous dispersion is acquired. Moreover, the ultrasonication period was divided into sequences of 3 sec on /1 sec off in order to prevent overheating due to the energy transferred by the ultrasonic waves. Ice cubes were also used for cooling down the samples during the process.

$$\phi_{vol} = \frac{1}{1+\left(\frac{1}{\phi_{wt}}\right)\left(\frac{\rho_{MWCNT}}{\rho_{Oil}}\right)} \tag{3.1}$$

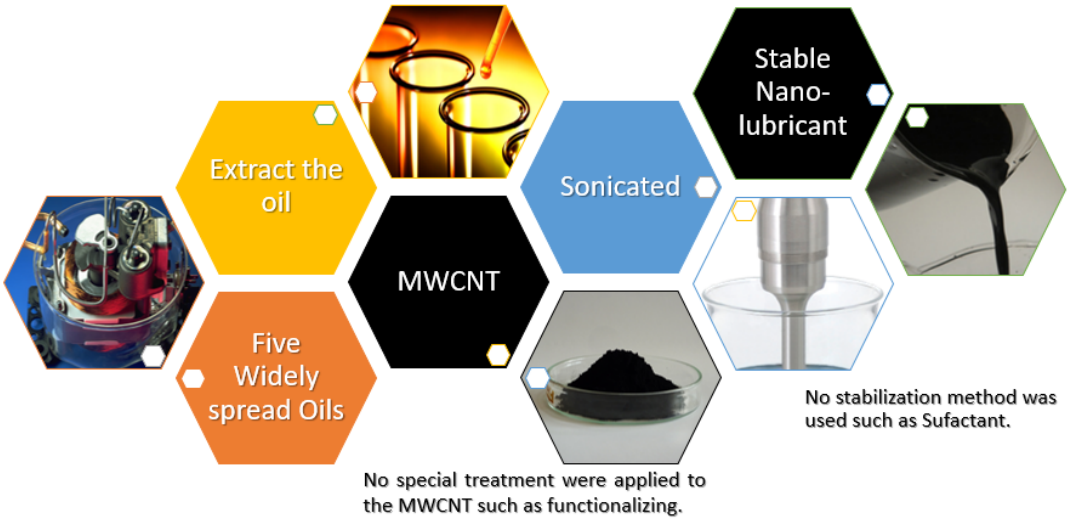

Figure 3.10 The steps of preparing the nanolubricants samples

Figure 3.11 The operated ultrasonic liquid probe-type processor (Sonicator 3000, MISONIX) for dispersing MWCNTs in oils

3.3 The Procedure of Measuring the Thermal Conductivity at Several Temperatures and Cancelling the Noise of the *1ω*

Before starting measuring the thermal conductivity of the nanofluid, a verification procedure should be first done in order to ensure that the measurement setup is ready to be utilized. Generally, the setup is verified by measuring known materials such as

water, Ethelyn Glycol, or mineral oil. If a deviation, above the acceptable error (normally ±0.5%) is realized, the wire should be checked if it is damaged, corroded or nanoparticles stick to it, as seen in Figure 3.10. Moreover, the 1ω signal which acts as a noise should be also double checked and cancelled before each measurement.

Now, after checking the steadiness of the setup, a nanofluid sample can be deployed. After immersing the probe inside the sample, it is recommended to wait for a couple of minutes before cancelling the 1ω signal and initiating the measurements until the temperature of the wire gets equalized with the temperature of its surrounding fluid. Ignoring this step will cause disturbance in the signal due to the effect of changing the temperature of the wire on the $V_{1\omega}$ and $V_{3\omega}$, as discussed in Chapter two. This also can be realized as fluctuation in the amplitude and the phase of the 3ω signal voltage.

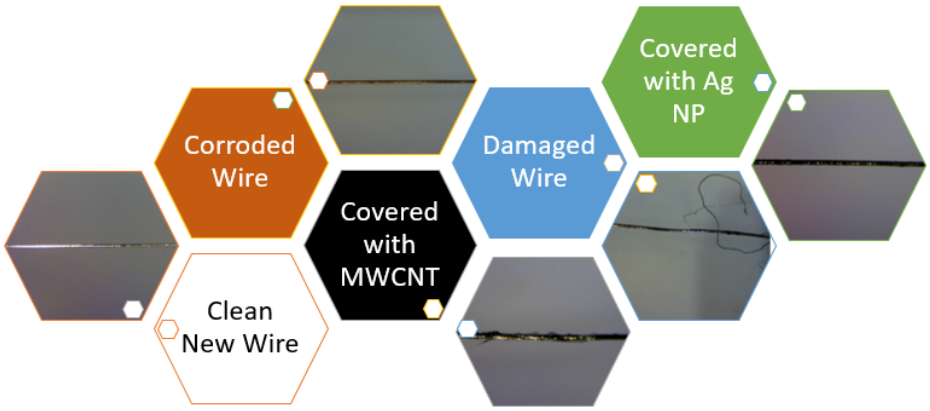

Figure 3.12 Comparison between a clean wire and other corrupted used wires after multi usages (Personal archive, 2017)

For the case of measuring the thermal conductivity at different temperatures, the temperature of the sample should be stabilized before initiating the measurement and cancelling the 1ω signal. Moreover, the thermal conductivity of the nanofluid should be measured relatively to its base fluid at the same temperature (Equation 2.37). Otherwise, the resulted ratio is wrong due to the notable change in the voltage components of the $V_{1\omega}$ and $V_{3\omega}$ due to the temperature change effect.

CHAPTER FOUR
RESULTS AND DISCUSSIONS

4.1 Stability and Re-dispersion Ability of the MWCNTs

Most of the available studies agreed that the main disadvantage of CNTs is their poor dispersibility in the common fluids, especially in water. Therefore, many chemical and mechanical approaches have been proposed to overcome this disadvantage: chemical methods involve using surfactants (Bystrzejewski et al., 2010; Li, Church, Kafi, Naebe, & Fox, 2014; O'Driscoll et al., 2014), functionalization the tubes to change their surface energy (Cao, Qiu, Yang, Chen, & Liu, 2014; Dong Kim, Park, & Lee, 2008; Ma, Siddiqui, Mäder, & Kim, 2011; Soulie-Ziakovic, Nicolay, Prevoteau, & Leibler, 2014; Wei et al., 2015; Zhang et al., 2015), improving their wetting characteristics (Dresel & Teipel, 2016) and reducing their tendency to agglomerate in the continuous phase solvent; mechanical methods collaborate mainly with adjusting grinding (Munkhbayar et al., 2012) or ultrasonication power and duration (Wu & Mitra, 2014; K. Yang et al., 2013). However, both methods can either seriously damage the structure of the CNTs, reshape their aspect ratio, or affect their surfaces resulting changes in the characteristic of their dispersions.

The unique structure of the carbon nanotubes turns their dispersion process into a challenge; the extremely high aspect ratio with the high flexibilities in addition to the Van der Waals attraction forces between the surfaces of the tubes dramatically increase the possibility of agglomeration and entanglement (Hilding et al., 2007). In addition to that, the medium where the tubes are dispersed in also plays a big role in this process. For example, it has been confirmed that the CNTs cannot be dispersed in water under normal conditions because of their hydrophobic nature (Devendiran & Amirtham, 2016). However, in the presented case, a relatively short time of ultrasonication was enough to get a homogenous MWCNTs/mineral oil suspension without adding any surfactant or using any special treatment to the tubes as shown in Figure 4.1 (b) due to the oleophilic property of MWCNTs as it will be discussed later. Moreover, it was surprising to realize that with any minor motion, done to the agglomerated samples, the sediment carbon nanotubes start to float and hold within the oil, as Figure 4.1 (d,

e, and f) illustrate. Furthermore, after well shaking (manually), it seems that we were able to fully re-disperse the agglomerated MWCNTs in oil Figure 4.1 (g).

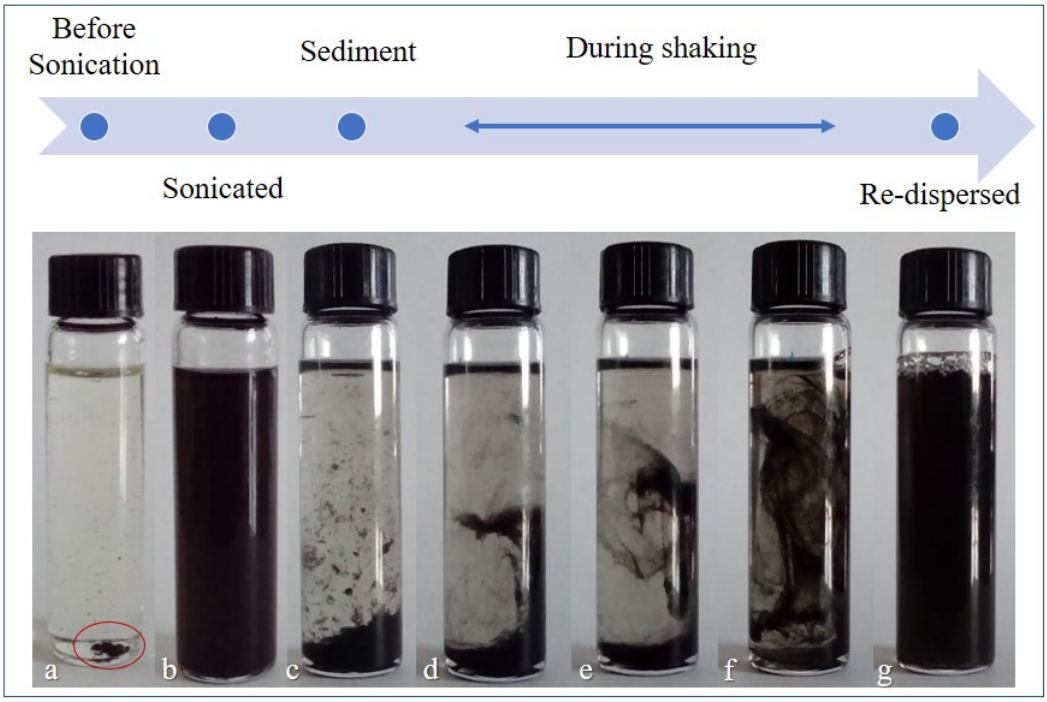

Figure 4.1 MWCNTs/Oil samples; (a): before Ultrasonication, (b): Ultrasonicated, (c): Sediment, (d)(e)(f): floating MWCNTs during shaking and (g): Re-dispersed (Fully shaken sample) (Personal archive, 2017)

To quantitatively ensure that the MWCNTs are fully re-dispersed, the particle size distribution (PSD) of the suspension was analyzed. The PSD measurement of the first sample was taken directly after ultrasonication, yet it has been waited for 21 days (to be sure the MWCNTs are fully agglomerated), then the sample were well shaken and deployed for measurement. In order to ensure the accuracy of the data, each measurement was repeated for 5 times and their mean values were calculated and presented in Figure 4.2 The graph reveals that the both samples have similar PSD trend; however, a slight shift in between is realized. The main peak of the recently sonicated suspension is at 993.4 d.nm with 34.4% intensity. The re-dispersed sample, on the other hand, shows a peak at 1110 d.nm with intensity of 36.7%. This small difference could be due to several reasons such as measurements accuracy, preparation conditions, partial agglomeration, or due to the different orientations of the tubes in

the front of the laser since we are not working with spherical particles. The cylindrical shape of the MWCNTs also attributes to give wider distribution (Tantra, Schulze, & Quincey, 2010) and the mean value of the PSD also to appear in the micro level since the length of the used MWCNTs is in the range of 10 to 30 µm.

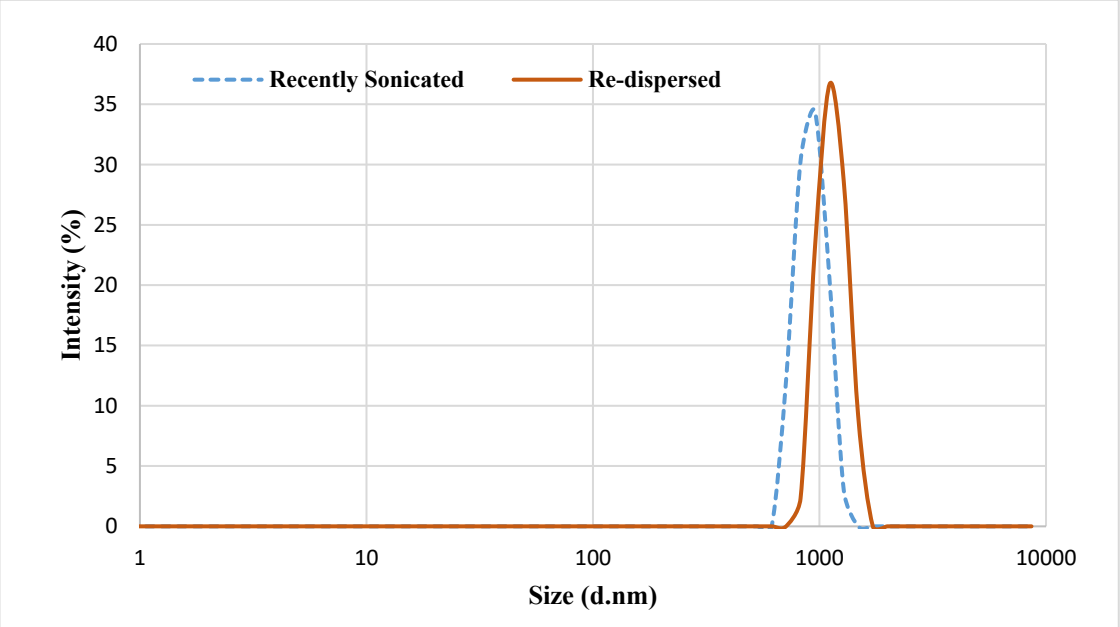

Figure 4.2 Comparison of PSD between the recently sonicated and re-dispersed MWNTs/low viscous oil suspensions; The X axis shows the distribution of size classes, while the Y axis shows the relative intensity

The main way to understand the re-dispersion ability of the MWCNTs starts from understanding the main reasons behind the ease of their dispersibility in oil comparing with water or any other base fluid. The ease of MWCNTs dispersibility in oil can be attributed to two reasons. First, the CNTs were found to be super-oleophilic (have very high affinity to oil) as Lee et al. (Lee, Johnson, Drelich, & Yap, 2011) and Fard et al. reported (Kayvani Fard, Mckay, Manawi, Malaibari, & Hussien, 2016). This property gives the researchers the chance to employ CNTs in manufacturing oil-water filters (Huang et al., 2016; Lee et al., 2011). In addition to that, CNTs were also utilized to create a sponge which can enormously absorb oil from water (Hashim et al., 2012). Consequently, during ultrasonication, it has been realized that the volume of the added amount of MWCNTs is enormously expanding. This means ultrasonication not only separate, disperses and covers the MWCNTs with oil, but it also enhances their ability

to adsorb it. This can be observed clearly from Figure 4.1; notice the difference in the volume of the MWCNTs in the case of the fully sediment suspension (c) and the case before ultrasonication (a). Second, Ettefaghi et al. (Ettefaghi et al., 2013) and Beheshti et al. (Beheshti et al., 2014) observed that when MWCNTs are dispersed in oil, they are placed between the oil layers which leads to ease the movement of these layers on each other. This leads to slightly lower the nanolubricant's viscosity than of the pure oil at low concentrations as they concluded. From this, we can also conclude that not only the MWCNTs ease the movement of oil layers on each other, but also the oil layers ease the movement of MWCNTs between them.

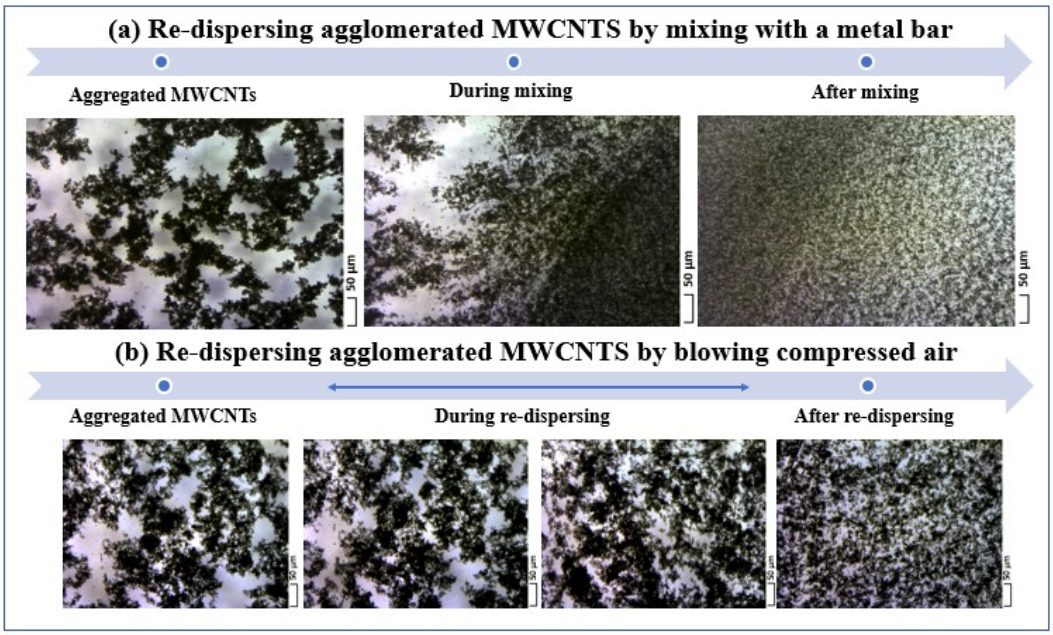

Figure 4.3 Optical microscope images of MWCNTs during redispersion within oil by (a) mixing with a metal bar and (b) blowing compressed air. The full redispersion process is presented in the attached video in the appendix (Personal archive, 2017)

According to the DLVO theory (Horinek, 2014), which is an essential theory to explain the stability of colloids in a suspension, the strong attraction force of Van der Waals acts on the very large surface area of the suspended MWCNTs. The MWCNTs, therefore, start to aggregate, which forms growing clusters as the times goes on. Large clusters sediments and accumulate above each other due to the effect of the gravitational force. The Van der Waals attracting force is inversely proportional to the fifth power of the distance between two interacting cylindrical particles (Hunter,

2001). To enhance the stability of a suspension, the distance between the particles should be increased. Conventionally, this can be done by enhancing the repulsive electrostatic force by increasing the energy barrier by changing the ionic, pH or adding surfactants to affect the surface charge of the colloid (Horinek, 2014). However, for the current studied nanolubricant, the MWCNTs are saturated and covered with oil layers which create barriers that can counterbalance the Van der Waals force by keeping distance between the tubes. Agitation, shaking or even blowing compressed air was realized to be able to break down the aggregations of the MWCNTs. The microscope images, given in Figure4.3 and the video in the Appendix, show that MWCNTs are detaching and floating in the oil during applying any slight force on the agglomerated suspension such as blowing compressed air. Floating MWCNTs, as also illustrated in Figure 4.1 (d-f) during shaking-stopping sequences, indicate that even after agglomeration the MWCNTs are still saturated and covered with oil. It is important to mention here that in each taken photo of Figure 4.1 (d-f) the floating tubes are holding in oil for hours.

The thickness of the separation oil layers is related to the viscosity of the base oil. An up to one month stability was reported (Ettefaghi et al., 2013; Ilyas et al., 2017), with high viscous oils by just ultrasonication. For the studied nanolubricants, both the recently sonicated and the fully re-dispersed by shaking, 48 h was the duration for full sedimentation as shown in Figure 4.1 (c). The low viscosity of the used oil, which is at least 10 times lower than of the oils used in the other investigations, can explain the relatively short duration of the stability.

To conclude in few words, the sonicated MWCNTs are separated, lubricated, saturated, and surrounded by oil layers, which not only ease its motion within the lubrication oil, but also create barriers between their surfaces that overcome the attraction force of Van der Waals, and as a consequence, give them the ability of detaching by applying any slight force.

4.1.1 Stability of the Re-dispersion Ability with Time

The influence of time on the re-dispersion ability can be reflected as a decaying in size quality after each re-dispersion process of the deagglomerated MWCNTs comparing to their first state after ultrasonication. It can also be revealed as a dramatic decrease in the thermal conductivity and viscosity due to the coexistence of the obsolete clustered tubes inside the nanolubricant. To inspect that, an ageing study was initiated on fully re-dispersed samples (by shaking) after resting times of 2, 10, 20 and 300 days since the first ultrasonication. Particle size distribution (Amiri et al., 2015), viscosity and thermal conductivity measurements were performed on the samples with the same procedures that were followed previously.

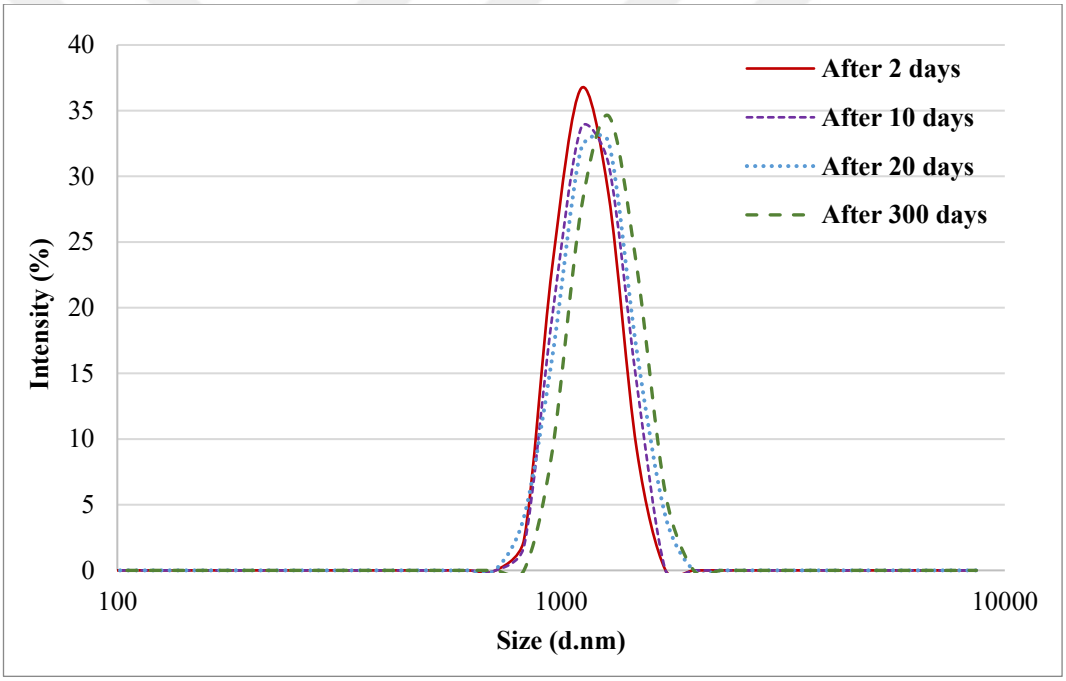

Figure 4.4 PSD comparison of fully re-dispersed MWNTs/low viscous oil suspensions by shaking after 2, 10, 20 and 300 days

Figure 4.4 represents a comparison between the particle size distributions of the examined samples at the considered intervals. As the plots illustrate, a slight trend toward larger particle size can be noticed. This shift can be observed more clearly by declaring the Z-average size as 1123,1147, 1171, and 1247 d.nm of each fully re-dispersed suspension after 2, 10, 20 and 300 days, respectively. The numbers and the graph imply that a minority of MWCNTs start to losses their ability for re-dispersing

and their quantity increases slowly with time. The main reason behind this behavior can be attributed to the decaying thickness of the oil layers between the sediment MWCNTs. The sediment tubes accumulate above each other for a long period of time. This give time to their surfaces to be attracted to each other due to the effect of Van der Waals' force and the supportive role of the gravitational force. As a consequence, the thickness of the separating oil layer become thinner and thinner until a point the tubes are not detachable anymore. The measurements of thermal conductivity and viscosity, on the other hand, did not reveal any difference between the tested samples. This means the obsolete MWCNTs minority did not affect noticeably the total homogeneity of the re-dispersed suspensions. Consequently, the thermal conductivity and the viscosity of the re-dispersed nanolubricant can be considered stable at least up to 300 days.

4.1.2 Thermal Conductivity as an Evaluation Criterion of The Re-dispersed Samples

The thermal conductivity of a nanofluid highly affected by the stability of the nanoparticles suspended within it. Consequently, any occurred agglomeration is reflected as a decline in the thermal conductivity. When the aggregation starts, the particle size increases resulting a decrement in the total surface areas of nanoparticles. The less surface area, thus, decreases heat transfer rates between the particles (Marquis & Chibante, 2005). Therefore, "Fluids with solid particles on a nano scale show better thermal conductivities than fluids with coarse solid particles on a micro scale" as Liu et al (M. Liu et al., 2011) stated. Depending on that, the thermal conductivity of the recently ultrasonicated and the re-dispersed samples were measured and compared at the room temperature with the respect of several weight concentrations. Identical enhancement ratios of the both samples were obtained within the error range. These ratios, as shown in Figure 4.29, are 1, 1.7, and 5% for 0.05, 0.1, and 0.3 wt.%, respectively. By aligning these ratios with the values of the existing investigations, it is noticed that they are among the lower ones. This divergence could be attributed to the type of the oil, characteristics of the used MWCNTs, preparation techniques, method of measurements, functionalizing the tubes and adding different surfactants, which were avoided for the aim of this investigation as discussed previously.

4.1.3 Viscosity as an Evaluation Criterion of the Re-dispersed Samples

The viscosity of a nanofluid and its stability with time and temperature are of great importance for any heat transfer application. Strong Van der Waal's force, as mentioned previously, causes an attraction between the tubes, which results with time MWCNTs clustering and thus inhomogeneity in the nanofluid. This inhomogeneity, as shown in the microscope images Figure 4.3 and in Figure 4.1 (c), can be realized as a higher or lower viscosity than of the homogeny nanofluid. Based on that, the changes in viscosity with temperature were evaluated for both fresh and re-dispersed samples at several weight concentrations. Measurements for fresh samples were taken directly after ultrasonication. However, for the re-dispersed ones, it has been waited for full sedimentation and then they were measured after well shaken. The obtained results, as shown later in Figure 4.20, indicate that the recently sonicated and re-dispersed samples at all concentrations give equal values within the uncertainty of measurements, which mean that MWCNTs are well re-dispersed within oil.

4.2 Thermal Conductivity Measurements with Respect to Temperature

This section emphases on the thermal conductivity measurements of pure and nanolubricants at different temperature. It also concerns about the effect of temperature on the thermal conductivity of the nanolubricant and the behavior of the MWCNTs inside their base fluid.

4.2.1 Validation of the 3ω Experimental Setup

In order to validate the utilized 3ω experimental setup, thermal conductivity measurements were performed on pure samples of ethylene glycol and mineral oil relatively to water with respect of temperature. The obtained results, as presented in Figure 4.5, indicate, as expected, that the thermal conductivity of ethylene glycol increases slightly with temperature. The thermal conductivity of oil, however, decreases by increasing its temperature. These obtained trends can be also confirmed by Figure 4.6.

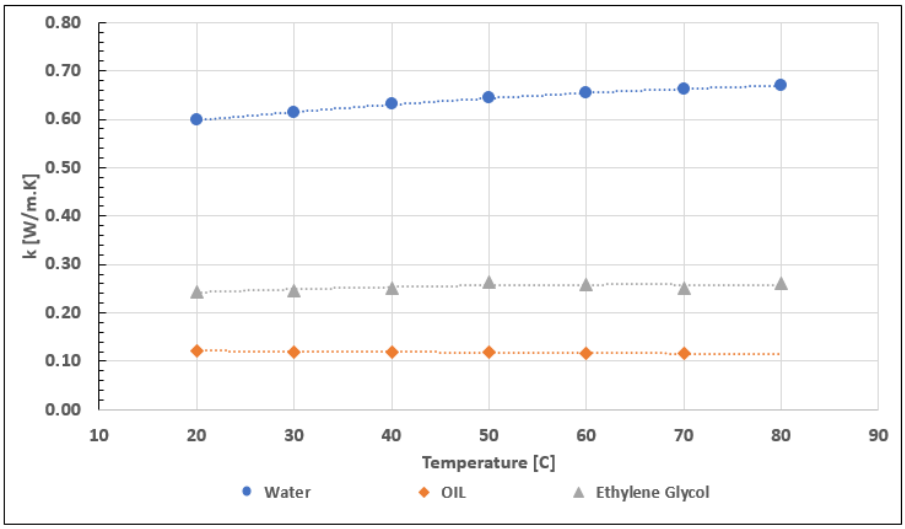

Figure 4.5 Thermal conductivity measurements of ethylene glycol and Mineral Oil relatively to water

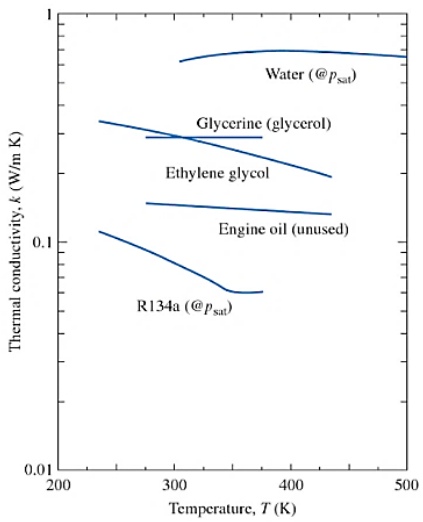

Figure 4.6 Thermal conductivity of several fluids with the respect of temperature (Kreith, Manglik, & Bohn, 2012)

Quantitively, the measured thermal conductivity of ethylene glycol was compared with the ones reported by (Bohne, Fischer, & Obermeier, 1984), as presented in Figure 4.7. The chart shows that both graphs have same trend. However, the thermal conductivity of the measured sample seems to trend higher with temperature. The maximum deviation reaches up to 2.8% in the respected temperature range. This slight deviation can be contributed mainly to the purity and the texture of the material since they were not purchased from the same source.

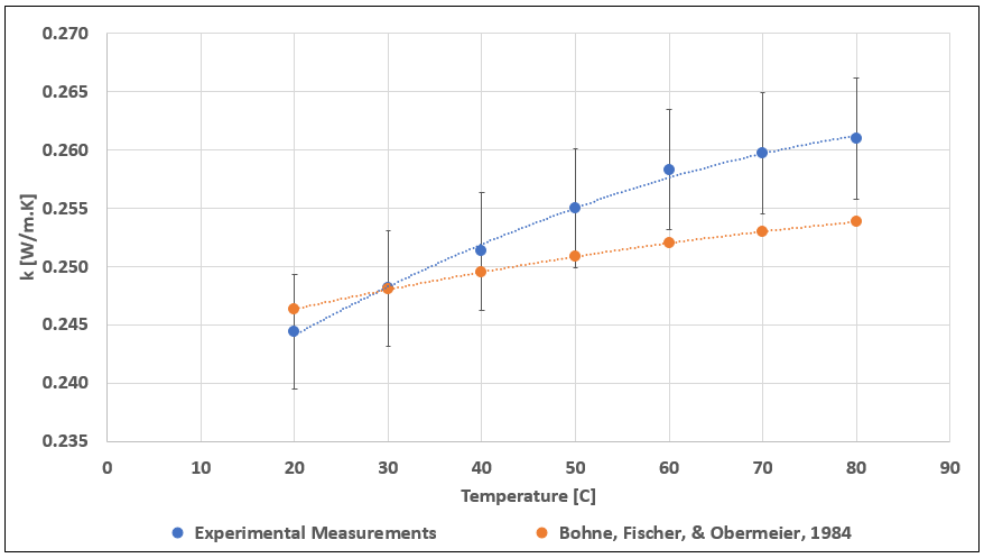

Figure 4.7 Comparison between the measured and reported thermal conductivities of ethylene glycol

Similarly, the thermal conductivity of the mineral oil is compared with several reported results (Antoniadis et al., 2016; Dombek, Nadolny, & Przybyłek, 2014; Nadolny, Dombek, & Przybylek, 2016; Wang et al., 2014). As Figure 4.8 reveals, the thermal conductivity of all considered and measured mineral oils decreases linearly with temperature. Furthermore, the thermal conductivities of the mineral oils are shifting above each other depending on their additives and composites.

Consequently, and based on the previously given results, the proposed lab-made 3ω setup can be considered reliable for measuring the thermal conductivity of a fluid at different temperatures.

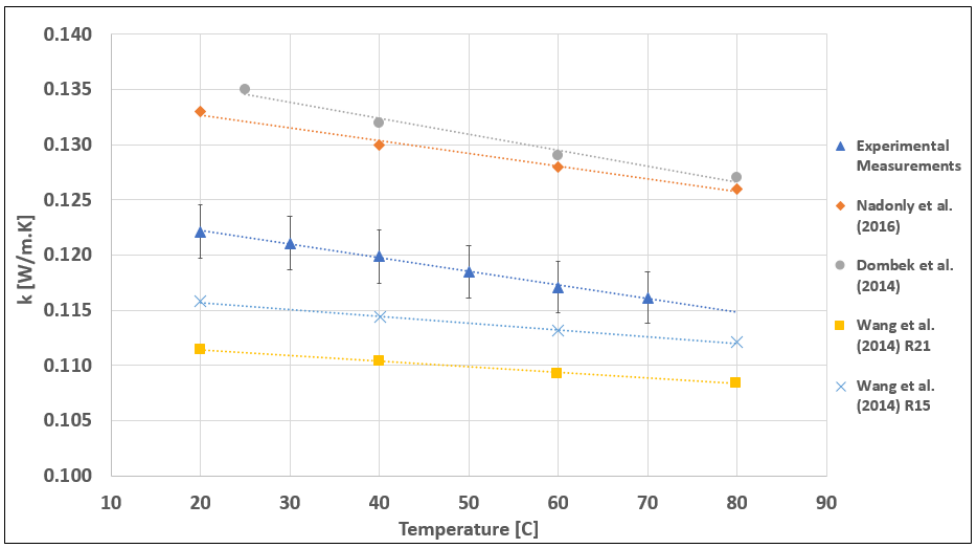

Figure 4.8 Comparison between the measured and reported thermal conductivities of mineral oil

4.2.2 Effect of Temperature on the Thermal Conductivity of MWCNTs Nanolubricants

After verifying that the measurement setups can be utilized for measuring thermal conductivity at several temperatures, the samples of the studied nanolubricants were deployed for measurements. Figures 4.9 to 4.15 present the thermal conductivity enhancement ratios (k_{nf}/k_{bf}) of the MWCNTs nanolubricants at 0.05, 0.1 and 0.3 wt.% with respect to temperature. The charts are ordered according to the viscosity of the base oil from the lowest to the highest.

Two main points can be realized from the presented figures. First, the enhancement in the thermal conductivity for all nanolubricants increases with the increment of MWCNTs' weight concentrations, as all of the other studies have also reported (Amiri et al., 2015; Beheshti et al., 2014; Chen & Xie, 2009; S. U S Choi et al., 2001; Ettefaghi et al., 2013; Fontes et al., 2015; Ilyas et al., 2017; Marquis & Chibante, 2005; Shaikh et al., 2007; Xie et al., 2003; Yang et al., 2006). The enormously higher thermal conductivity and the very larger specific surface area of the MWCNT, as believed, are the main reason behind the increment (Liu et al., 2005).

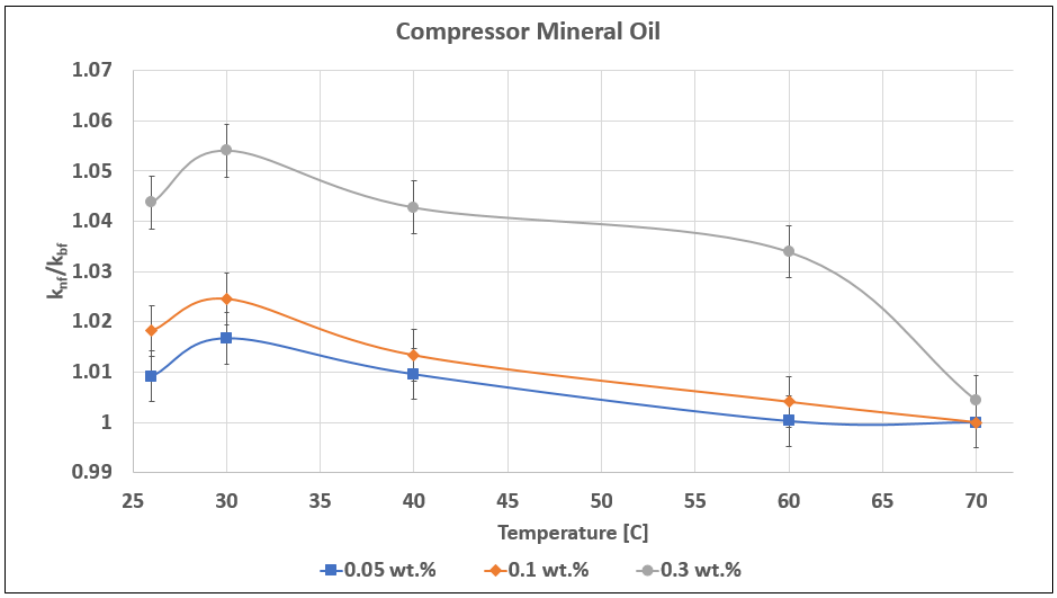

Figure 4.9 Thermal conductivity enhancement ratios of MWCNT/Compressor mineral oil at several weight concentrations with respect to temperature

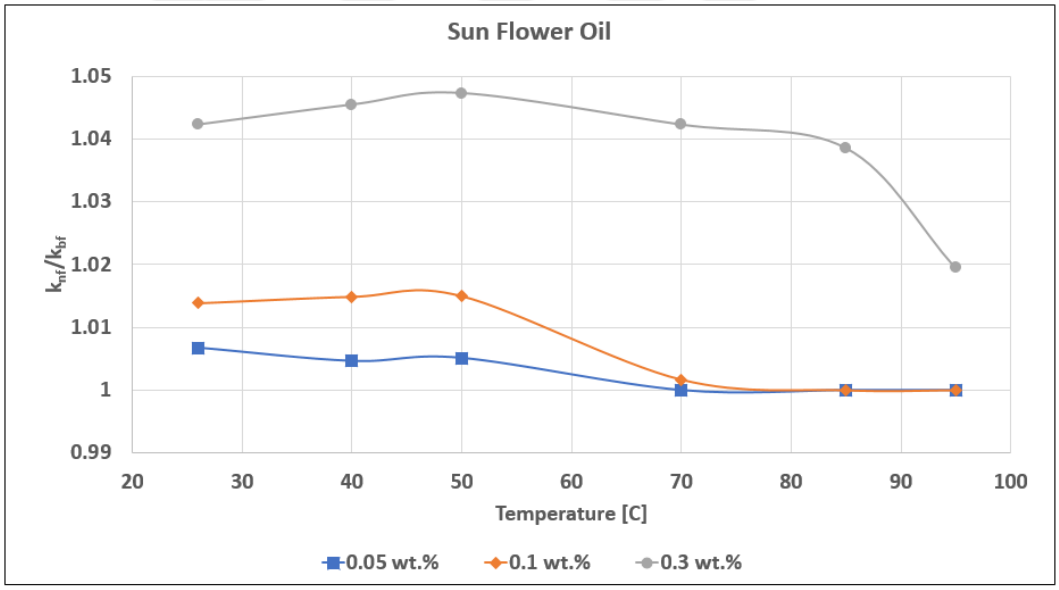

Figure 4.10 Thermal conductivity enhancement ratios of MWCNT/Sunflower oil at several weight concentrations with respect to temperature

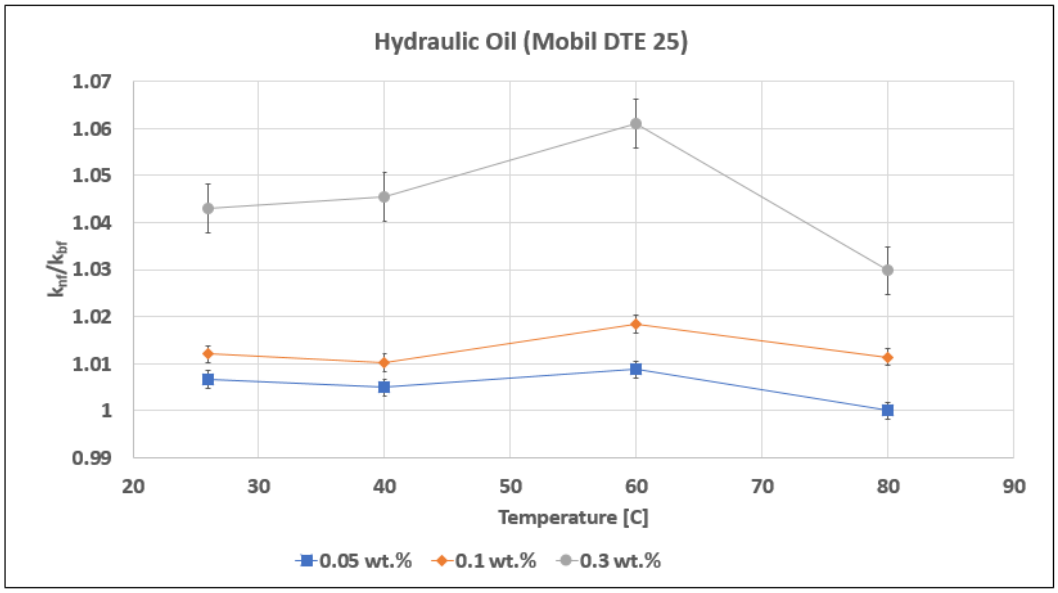

Figure 4.11 Thermal conductivity enhancement ratios of MWCNT/Hydraulic oil (Mobil DTE 25) at several weight concentrations with respect to temperature

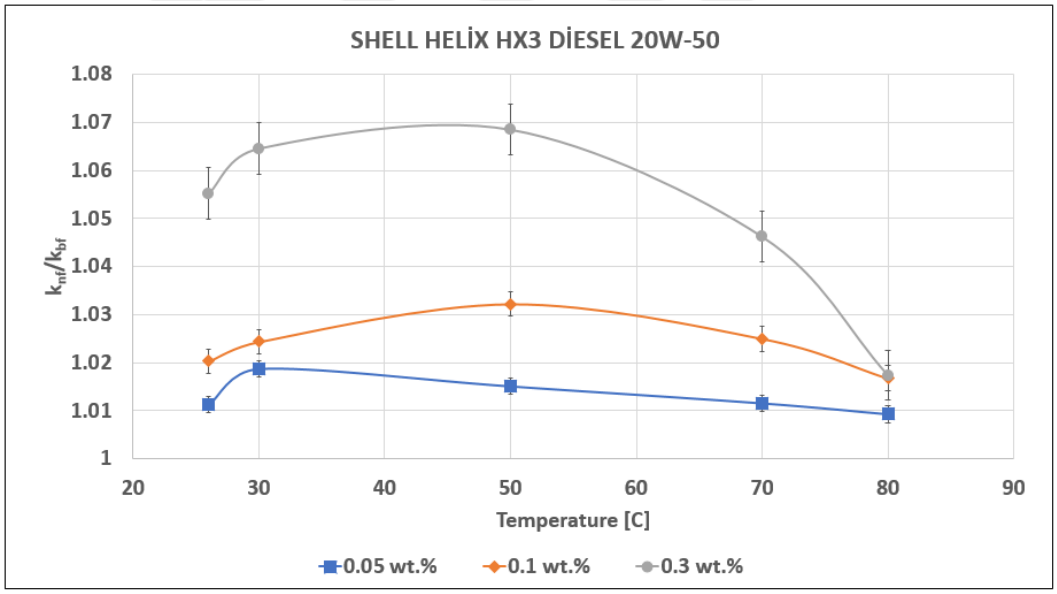

Figure 4.12 Thermal conductivity enhancement ratios of MWCNT/Shell (Helix HX3 DIESEL) oil at several weight concentrations with respect to temperature

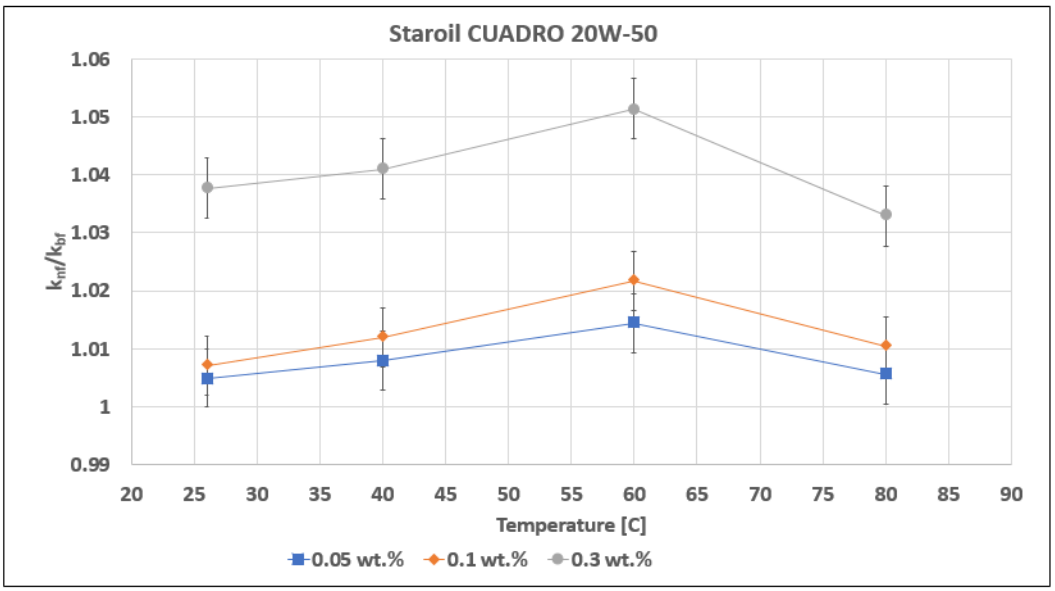

Figure 4.13 Thermal conductivity enhancement ratios of MWCNT/Star Oil (CUADRO 20W-50) at several weight concentrations with respect to temperature

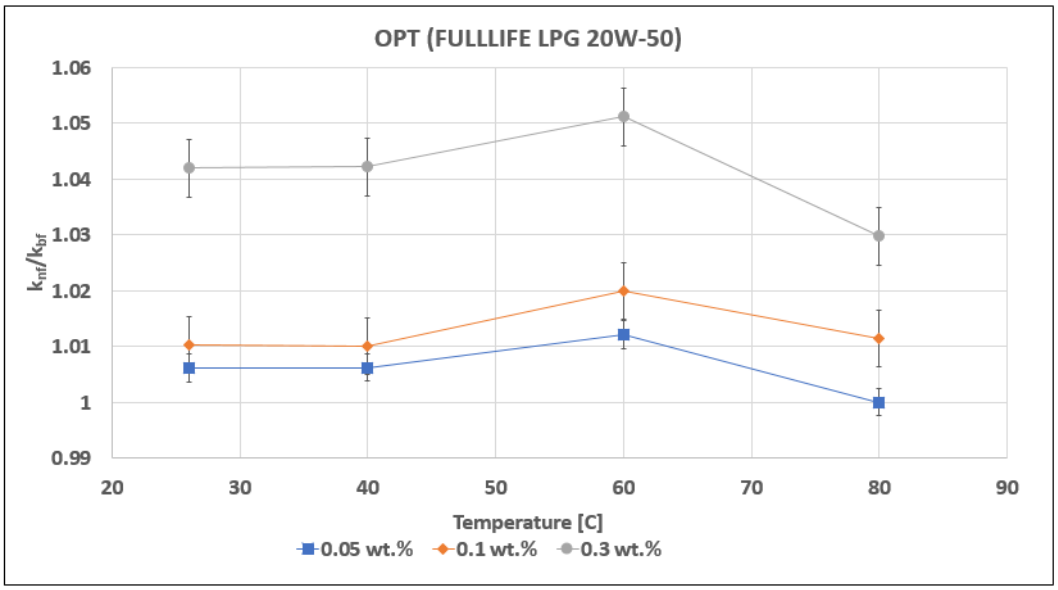

Figure 4.14 Thermal conductivity enhancement ratios of MWCNT/OPT (Full life LPG 20W-50) at several weight concentrations with respect to temperature

Moreover, six possible main mechanisms are offered to explain the heat conduction in nanofluids according to Wang et al. (Wang et al., 2012). Among them, clustering of nanoparticles and nano layering of the liquid at the liquid/nanoparticle interface are more likely responsible for increasing the thermal conductivity of the investigated nanolubricant. First, the dispersed MWCNTs can form, by clustering, an extensive

network. This network facilitates thermal bridges within the base fluid as shown in the microscope images, Figure 4.3. Therefore, increasing the MWCNTs weight concentration will increase the chance of constructing more intensive thermal bridges network. Second, the oil layers, structured near the tubes as discussed before, have significantly lower thermal conductivity than of the MWCNTs. These layers work relatively as a thermal isolation between the tubes. The thickness of these layers, which, depends on the viscosity of the oil, play a notable role in the heat transfer rate between the tubes. This reason can possibly explain why the enhancement in the nanolubricants was not as high as expected in other base fluids.

Furthermore, it can be also noted from the graphs that the relative enhancement ratios of all nanolubricants are very close to each other when they are compared at each weight concentration. The main reason behind this behavior can be contributed to the fact that the thermal conductivities of the base fluids are also close to each other, as it can be observed from Figure 4.16. The oil layers, as stated previously, contribute to the heat rate between the tubes. Consequently, similar thermal conductivities will lead to relatively similar enhancement ratios and vice versa.

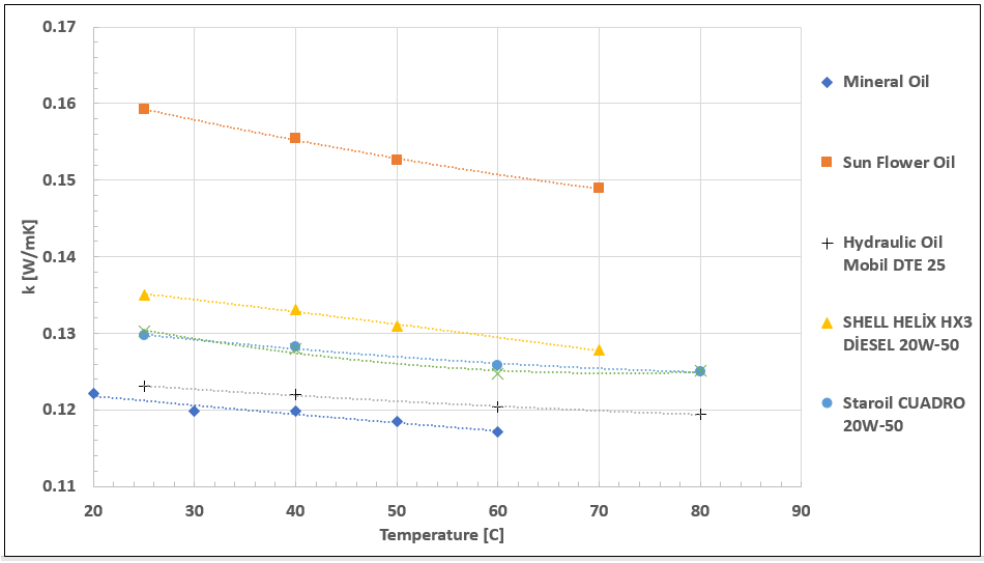

Figure 4.15 Thermal conductivities of the base oils with respect to temperature

The second interesting phenomenon that can be observed from the graphs is that the thermal conductivity enhancement ratios tend to peak at a specific temperature and

then decay until they perish. In other words, the thermal conductivities of the nanolubricants reach maximum values at specific temperatures and then decrease until it reaches the value of the base oil.

In order to more clarify this behavior, samples of the nanolubricants were taken and heated until a constant temperature (80 ºC) under microscope, as Figure 4.17 and video 2 (See the supplementary material) show. At the beginning of the heating, nothing interesting, beside decrement in viscosity, was realized. However, after reaching a temperature at which natural convection currents appear, the MWCNTs start floating inside the oil and clustering. As the time goes on, the agglomeration of MWCNTs grows until it reaches a point after which the separation of MWCNTs can be recognized easily by the naked eye, as seen in Figure 4.17.

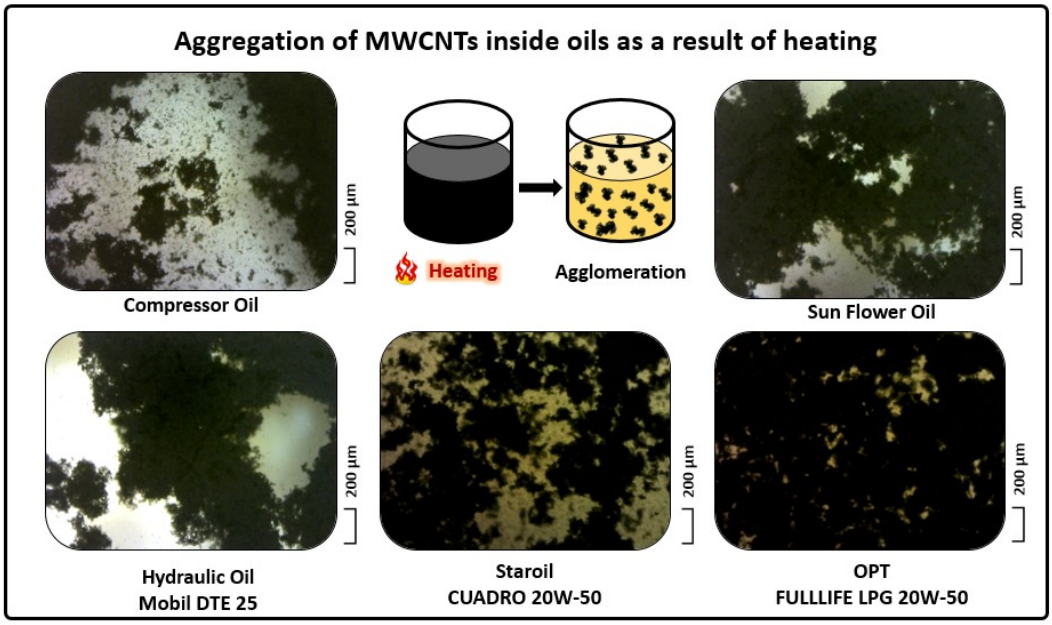

Figure 4.16 Aggregation of MWCNTs inside oil after heating the nanolubricant (Personal archive, 2017)

As it is well known, when the temperature increases the viscosity of the oil decays dramatically, as Figure 4.18 indicate. Decreasing the viscosity of the oil will thin the separation oil layers between the MWCNTs which, consequently, narrows the distance between them. At narrower distance, the magnitude of the Van der Waals forces rises which leads to increasing attraction between the tubes. With increasing the temperature, the oil layers become thinner and thinner until they totally disappear. At

that point the MWCNTs totally agglomerate within oil, as illustrated in Figure 4.19 and shown in Figure 4.17 and Video 2. Furthermore, the convection currents act as agitator that increase the possibility of contacting the floating MWCNTs with each other inside the oil.

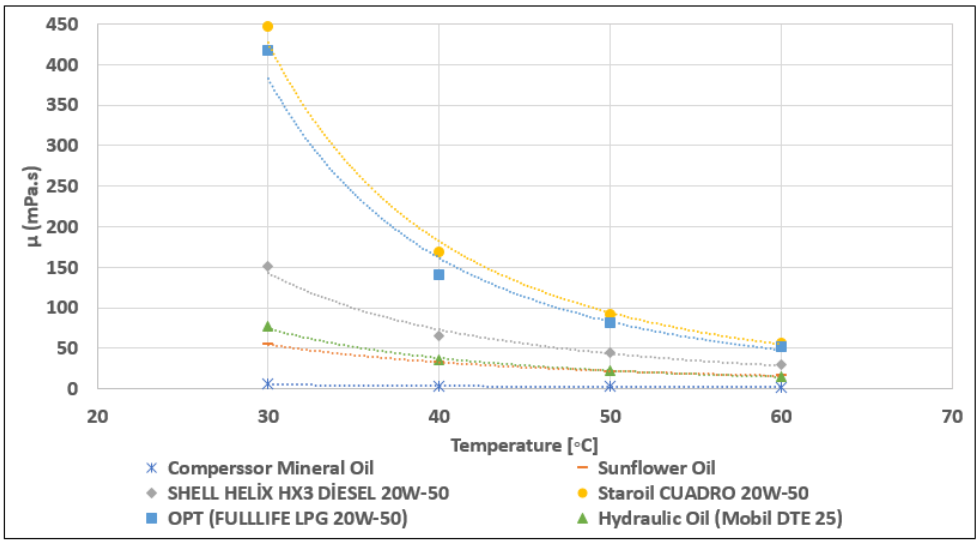

Figure 4.17 Dynamic viscosity of the pure base oils with respect to temperature

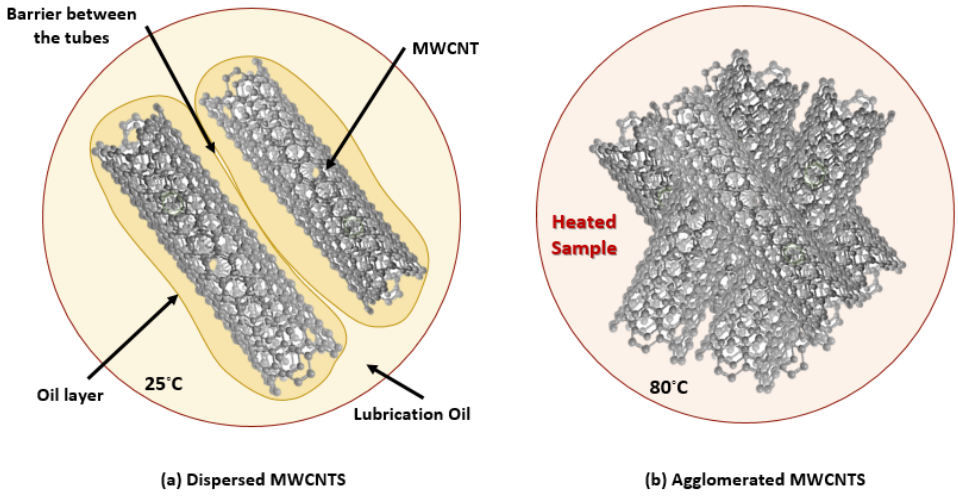

Figure 4.18 Illustration of MWCNTs behavior inside oil depending on temperature (a) Oil layers work as barrier that counter balance Van der Waals forces (b)Aggregation of MWCNTs inside oil after heating the nanolubricant

Out of 14 research papers (which have been discussed previously in the introduction), 4 reported the thermal conductivity of the MWCNTs nanolubricants

with respect to temperature and realized similar behavior. (Chen & Xie, 2009) stablized MWCNTs in silicone oil by mechanical ball mill technology and with the aid of concentrated acid treatment and hexamethyldisiloxane as dispersant and inspected its thermal conductivity, as shown in Figure 4.20 (a). Chen & Xie explained the increament of thermal conductivity with temperature as a result of the great decline of silicon oil viscosity which, consequently, improved the dispersing state of the MWCNTs. It worth mentioning here that the enhncment ratio here just increased without decaying. This can be more when the viscosity of their nanolubricants reached almost 200 mpa.S at 60 ºC. In more specific words, it does not reach the point at which the oil seperation barriers between the tubes disappears. Moreover, the role of the acidic treatment and the surfectant sould not be forregeten.

(Beheshti et al., 2014) reported the thermal conductivity of transformer oil-oxidized MWCNTs at different temperatures, as shown in Figure 4.20 (b). They observed that at higher temperature of 60 ºC, MWCNTs start to accumulate in the oil and the clustered tubes migrate toward zones of higher concentration. Their explanation of this phenomenon can be summarized that the main reason can be contributed to Brownian motion, thermophoresis and diffusiophoresis. They also claimed that electrical double layer (ELD) on the surface of the nanotubes can affect particles movement and their migration toward the opposite charge. It also important to mention here that the viscosity of the naonolubricants drops to 5 mPa.s at 60 ºC which is perfect for the MWCNTs to make contact with each other.

Amiri et al. (2015) also investigated the thermal conductivity of functionalized MWCNTs with hexylamine (HA) suspended in transformer oil. They also experienced increment in the thermal conductivity with temperature, as presented in Figure 4.20 (c). Based on that they stated that "*temperature plays a key role in increasing the thermal conductivity of MWNT–HA/TO coolant, which cannot be neglected*". Furthermore, they claimed that the problem of the settlement MWCNTs, which was previously reported by (Beheshti et al., 2014), was completely eradicated due to the functionalization of MWNT with HA. Actually, by solving this problem, they were able to break the 60 ºC barrier and record continuously higher thermal conductivities up to 80 ºC. The enhancement in the thermal conductivity of their nanolubricant was

contributed to the effect of the surface liquid nano-layer around the MWCNTs which exhibit higher thermal conductivity compared to the base oil. Moreover, they emphasized on the role of the Brownian motion of the tubes which increase with temperature due to the significant decrement in the viscosity.

Ilyas et al. (2017) realized that thermal conductivity of MWCNTs/thermal oil increases with temperature and particle concentration. They attributed this increament to Brownian motion and thermophoresis behavior of nanotubes. The thermophoresis behaviour is a process where particles moves from high toward low temperature zones. This similar to heat transfer mechanisim but for the case of particles (Quintiere, 2016). Nevertheless, the thermophoresis behaviour does not have that much effect in this case since the temperature of the measured medium is homogeneous and does not have temperature zones.

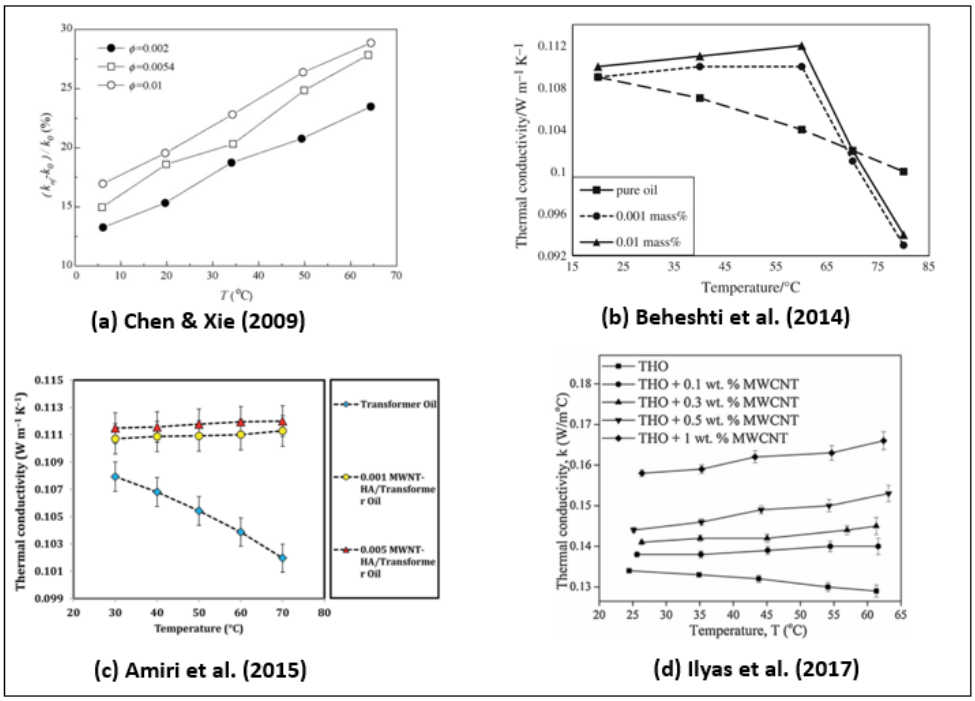

Figure 4.19 Thermal conductivities of MWCNTs nanolubricants reported in another related research paper

4.2.3 Effect of Temperature on the Viscosity of MWCNTs Nanolubricants

Figures 4.21 to 4.26 present the viscosity of the MWCNTs nanolubricants as a function of temperature and weight concentration. As the graphs illustrate, nanolubricants demonstrate here two behaviors. First, at a constant temperature, the dynamic viscosities of the low and medium viscous nanolubricants (Compressor mineral oil, Sunflower oil and Hydraulic oil) show notable enhancement with the increment of the MWCNTs weight concentration. This enhancement is more significant at lower temperatures. On the other hand, the viscosity of the high viscous engine oils (HELIX, OPT, and Staroil) decreases at low weight concentration (0.05 wt.%) and then increases with the higher concentrations. The enhancement in the viscosity is caused mainly due to the attraction between the MWCNTs which constructs a network of tubes within the base oil, as seen previously. The intensity of the tubes network becomes greater and greater with the increment of weight concentration. Nevertheless, within the high viscous oils, the MWCNTs are placed between the oil layers, as discussed previously. Moreover, the thickness of the oil separation layer increases notably due to the high viscosity of the surrounding medium. Consequently, at low concentration the MWCNTs are not able to construct effectively the tubes network. This leads that MWCNTs just ease the movement of these layers on each other due to their lubrication property and hence lower the viscosity of the nanolubricant. This phenomenon of the lubrication behavior of the MWCNTs within the base oil at low concentrations was first realized by Ettefaghi et al. (2013) and Beheshti et al. (2014), as discussed previously and mentioned previously.

Second, the dynamic viscosity of the nanolubricant decreases dramatically with the increase in temperature. This behavior is due to the decrease in viscosity of the base oil, which is a result of declining the intermolecular forces of the oil itself. Moreover, the agglomeration of the heated MWCNTs, as mentioned and discussed previously, also played a supportive role in this decrement.

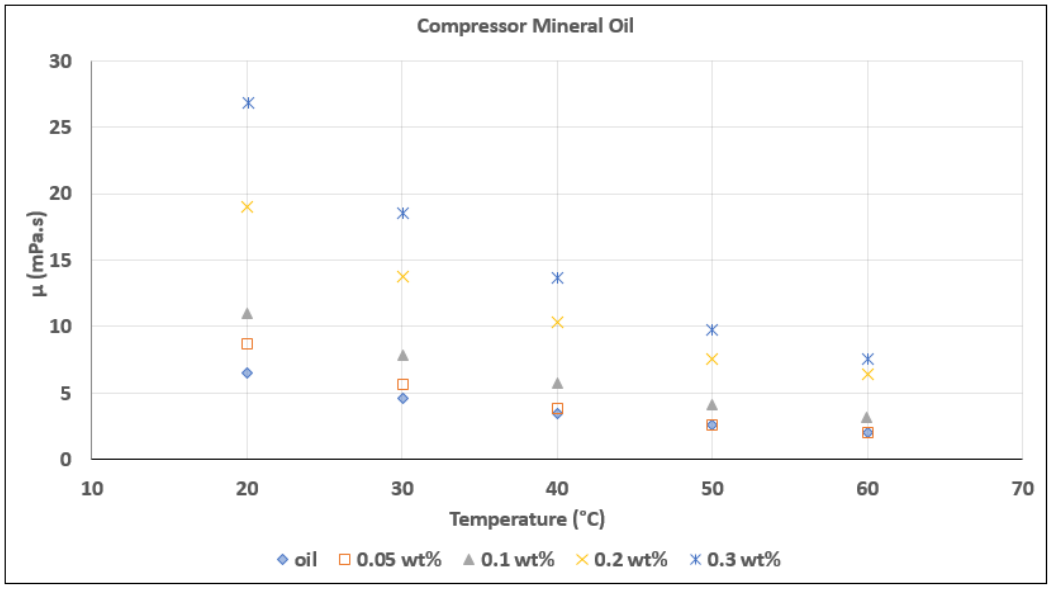

Figure 4.20 Dynamic viscosity of the MWCNTs/compressor mineral oil at different with concentrations with respect to temperature

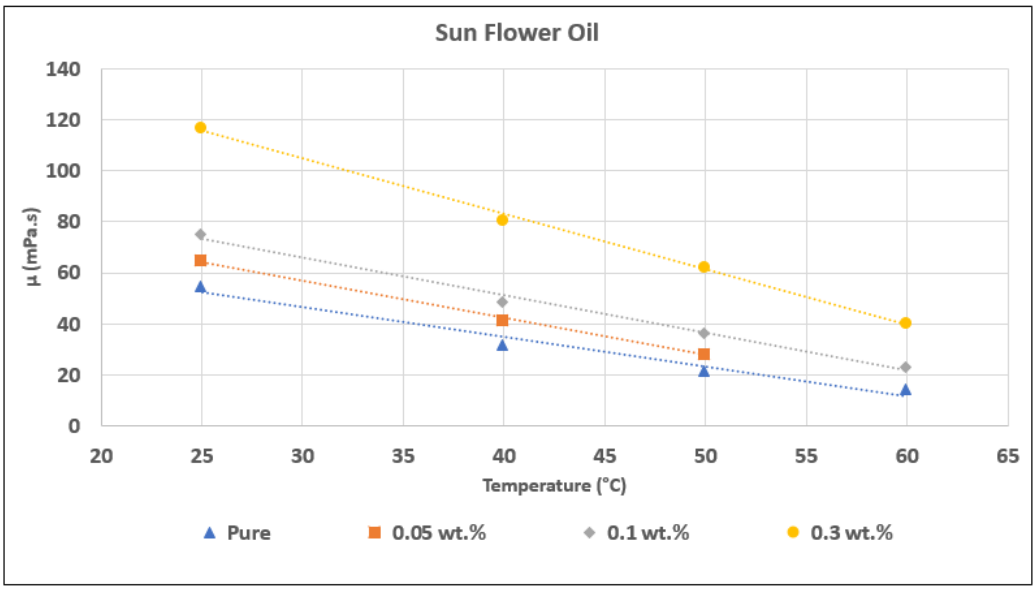

Figure 4.21 Dynamic viscosity of the MWCNTs/Sunflower oil at different weight concentrations with respect to temperature

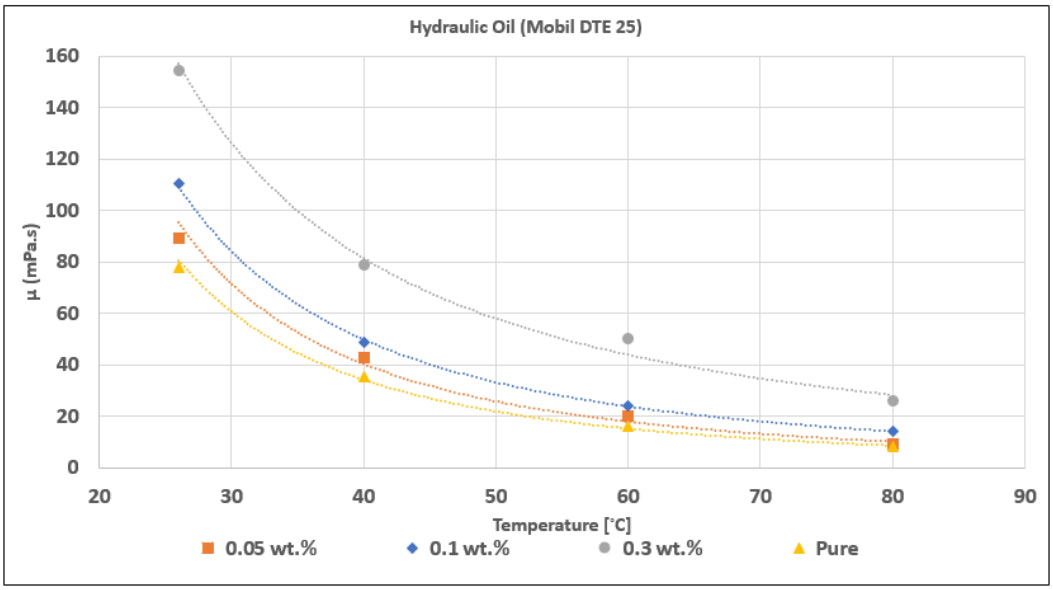

Figure 4.22 Dynamic viscosity of the MWCNTs/Hydraulic Oil (Mobil DTE 25) at different weight concentrations with respect to temperature

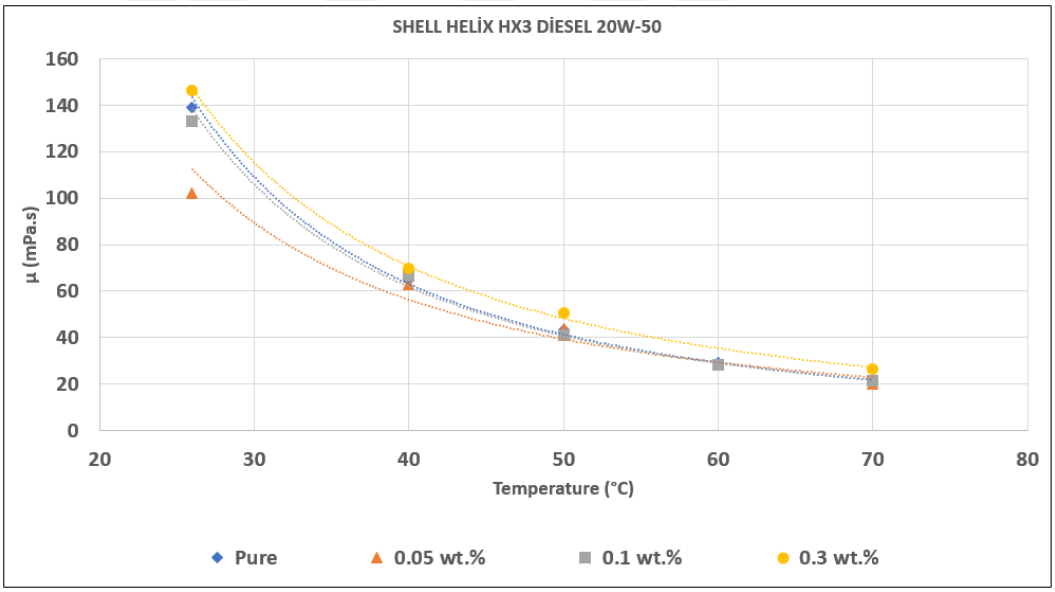

Figure 4.23 Dynamic viscosity of the MWCNTs/Shell Helix HX3 DIESEL 20W-50 at different weight concentrations with respect to temperature

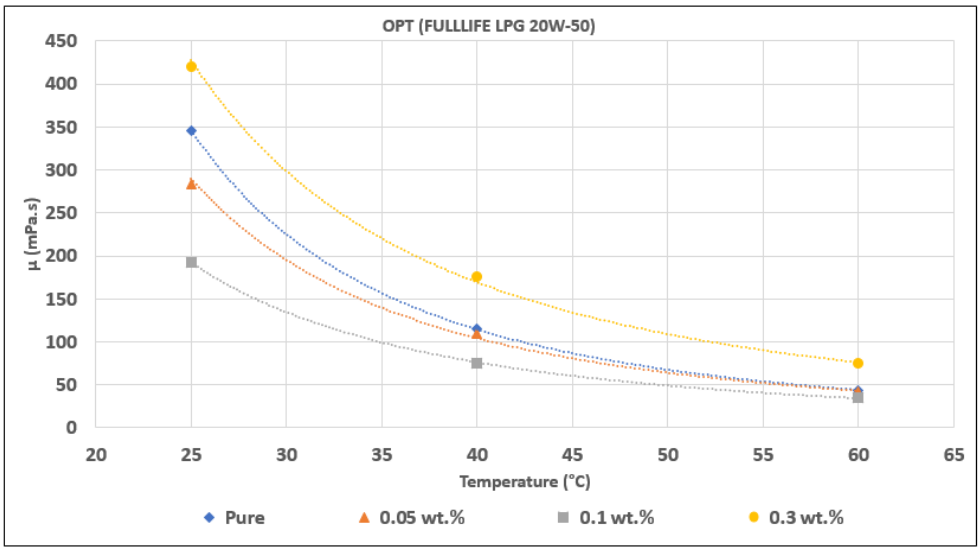

Figure 4.24 Dynamic viscosity of the MWCNTs/OPT (FULLLIFE LPG 20W-50) at different weight concentrations with respect to temperature

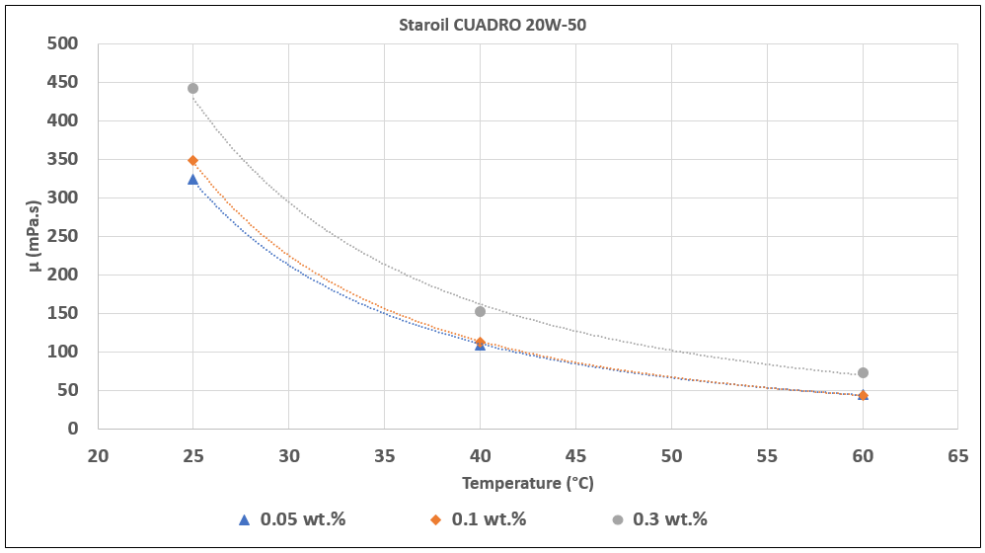

Figure 4.25 Dynamic viscosity of the MWCNTs/Staroil CUADRO 20W-50 at different weight concentrations with respect to temperature

CHAPTER FIVE
CONCLUSIONS

This research investigated the influence of temperature on the thermal conductivity of several MWCNTs nanolubricants and the ability of the sonicated MWCNTs of re-dispersing in low viscous oil. The main ideas of this work can be concluded in the following points:

- without any special treatment, MWCNTs were easily dispersed by ultrasonication within commercially well-known oil of several viscosities. Stable nanolubricants at several concentrations were obtained without using any stabilization method.

- The sonicated MWCNTs found to be separated, saturated, lubricated, and surrounded by oil layers, which ease its motion within the lubrication oil and create barriers between their surfaces. These separation layers counterbalance Van der Waals forces and give the MWCNTs the ability of detaching by applying any slight force. Microscopic video and images have proved that agitating, shaking or even blowing compressed air on the agglomerated nanolubricant breaks down the aggregation of the MWCNTs.

- The particle size distribution analysis indicates similar dispersion quality of the recently sonicated and the re-dispersed suspensions. Furthermore, the viscosity and thermal conductivity measurements give equal results, within the uncertainty of the measurement setups, of both suspensions at different weight concentrations. According to these obtained results, it has been confirmed that the MWCNTs are re-dispersible to the same degree of the recently sonicated ones by just shaking.

- The effect of changing temperature and the resulted transient zone, after which the system is re-stabilized, should not be neglected for cancelling the noise of the 1ω and measuring the amplitude and the phase of the 3ω signal.

- After cancelling the noise of the *1ω* at each temperature, the *3ω* method was found to be sufficiently reliable and accurate for measuring the thermal conductivity of different fluids with respect to temperature.

- Heating the MWCNTs nanolubricants to higher temperatures (60-80 ºC) resulted in agglomeration of MWCNTs. This was a result of the disappearance of the oil separation layers which leads to enhance the effect of the Van der Waals forces. Moreover, convection currents act as agitator which also enhance the contacts between the MWCNTs.

- Under the influence of temperature, which affects the thickness of the oil suppuration layers consequently, the thermal conductivities of the nanolubricants reach maximum values at specific temperatures and then decrease until it reaches the value of the base oil.

- Without the accuracy of the 3ω method it was impossible to sense the slight deviation in the thermal conductivity which leads to discover the realized behaviors of the MWCNTs within oils.

Consequently, it is observed that the temperature is an essential parameter for the stability, viscosity and thermal conductivity of the MWCNTs nanolubricants. Furthermore, heating nanolubricants resulted in MWCNTs clustering. Nevertheless, the sonicated tubes still acquired the re-dispersion ability by agitation. This lead to the following question: How will the MWCNTs nanolubricants behave in real life application such as engines? How will also adding a surfactant will affect these parameters. The answers of these question are left for future research works.

REFERENCES

Amiri, A., Kazi, S. N., Shanbedi, M., Zubir, M. N. M., Yarmand, H., & Chew, B. T. (2015). Transformer oil based multi-walled carbon nanotube-hexylamine coolant with optimized electrical, thermal and rheological enhancements. RSC ADVANCES, *5*(130), 107222–107236.

Antoniadis, K. D., Tertsinidou, G. J., Assael, M. J., & Wakeham, W. A. (2016). Necessary Conditions for Accurate, Transient Hot-Wire Measurements of the Apparent Thermal Conductivity of Nanofluids are Seldom Satisfied. *International Journal of Thermophysics*, *37*(8), 78.

Beheshti, A., Shanbedi, M., & Heris, S. Z. (2014). Heat transfer and rheological properties of transformer oil-oxidized MWCNT nanofluid. *Journal of Thermal Analysis and Calorimetry*, *118*(3), 1451–1460.

Birge, N. O., & Nagel, S. R. (1987). Wide-frequency specific heat spectrometer. *Review of Scientific Instruments*, *58*(8), 1464–1470.

Bohne, D., Fischer, S., & Obermeier, E. (1984). Thermal, Conductivity, Density, Viscosity, and Prandtl-Numbers of Ethylene Glycol-Water Mixtures. *Berichte Der Bunsengesellschaft Für Physikalische Chemie*, *88*(8), 739–742.

Borca-Tasciuc, T., Kumar, A. R., & Chen, G. (2001). Data reduction in 3ω method for thin-film thermal conductivity determination. *Review of Scientific Instruments*, *72*(4), 2139–2147.

Bystrzejewski, M., Huczko, A., Lange, H., Gemming, T., Büchner, B., & Rümmeli, M. H. (2010). Dispersion and diameter separation of multi-wall carbon nanotubes in aqueous solutions. *Journal of Colloid and Interface Science*, *345*(2), 138–142.

Cahill, D. G. (1990). Thermal conductivity measurement from 30 to 750 K: The 3ω method. *Review of Scientific Instruments*, *61*(2), 802–808.

Cahill, D. G., & Pohl, R. O. (1987). Thermal conductivity of amorphous solids above the plateau David, *Physical Review B*, *35*(8), 4067–4073.

Cao, Z., Qiu, L., Yang, Y., Chen, Y., & Liu, X. (2014). The effects of surface modifications of multiwalled carbon nanotubes on their dispersibility in different solvents and poly(ether ether ketone). *Journal of Materials Research*, *29*(22), 2625–2633.

Carslaw, H. S., & Jaeger, J. (1959). Conduction of Heat in Solids, 510 pp., Clarendon. Oxford, UK.

Chen, L., & Xie, H. (2009). Silicon oil based multiwalled carbon nanotubes nanofluid with optimized thermal conductivity enhancement. *Colloids and Surfaces A-Physicochemical and Engineering Aspects*, *352*(1–3), 136–140.

Chirtoc, M., & Henry, J. F. (2008a). 3ω hot wire method for micro-heat transfer measurements: From anemometry to scanning thermal microscopy (SThM). *European Physical Journal: Special Topics*, *153*(1), 343–348.

Chirtoc, M., & Henry, J. F. (2008b). 3ω Scanning Thermal Microscopy : New Theoretical Model and Validation by Lock-in Micro-Thermographic Temperature Mapping. *European Physical Journal: Special Topics, 153*(1), 343-348.

Choi, S. R., Kim, J., & Kim, D. (2007). 3ω Method To Measure Thermal Properties of Electrically Conducting Small-Volume Liquid. *Review of Scientific Instruments*, *78*(8), 1–7.

Choi, S. U. S., Eastman, J. A., & Chol, S. U. S. (1995). Enhancing thermal conductivity of fluids with nanoparticles. *ASME-Publications-Fed*, *231*, 99–106.

Choi, S. U. S., Zhang, Z. G., Yu, W., Lockwood, F. E., & Grulke, E. A. (2001). Anomalous thermal conductivity enhancement in nanotube suspensions. *Applied Physics Letters*, *79*(14), 2252–2254.

Corbino, O. M. (1911). Periodic variation of resistance of metallic filaments on alternating current. *Atti Della Reale Accademia Nazionale Dei Lincei*, *20*, 222–228.

Dames, C., & Chen, G. (2004). Theoretical phonon thermal conductivity of Si/Ge superlattice nanowires. *Journal of Applied Physics*, *95*(2), 682–693.

Dames, C., & Chen, G. (2005). 1Ω, 2Ω, and 3Ω Methods for Measurements of Thermal Properties. *Review of Scientific Instruments*, *76*(12), 1–14.

Devendiran, D. K., & Amirtham, V. A. (2016). A review on preparation, characterization, properties and applications of nanofluids. *Renewable and Sustainable Energy Reviews*, *60*, 21–40.

Ding, Y., Alias, H., Wen, D., & Williams, R. A. (2006). Heat transfer of aqueous suspensions of carbon nanotubes (CNT nanofluids). *International Journal of Heat and Mass Transfer*, *49*(1–2), 240–250.

Dombek, G., Nadolny, Z., & Przybyłek, P. (2014). The Study of Thermal Properties of Mineral Oil and Synthetic Ester Modified by Nanoparticles TiO 2 and C 60. *Ichve*, 1–4.

Dong Kim, S., Park, S., & Lee, Y. (2008). Chemical Surface Treatment for Highly Improved Dispersibility of Multi-Walled Carbon Nanotubes in Water. *Journal of Dispersion Science and Technology*, *29*(February 2015), 426–430.

Dresel, A., & Teipel, U. (2016). Influence of the wetting behavior and surface energy on the dispersibility of multi-wall carbon nanotubes. *Colloids and Surfaces A: Physicochemical and Engineering Aspects*, *489*, 57–66.

Ettefaghi, E.-I. o llah, Ahmadi, H., Rashidi, A., Nouralishahi, A., & Mohtasebi, S. S. (2013). Preparation and thermal properties of oil-based nanofluid from multi-walled carbon nanotubes and engine oil as nano-lubricant. *International Communications in Heat and Mass Transfer*, *46*, 142–147.

Evgin, T., Koca, H. D., Horny, N., Turgut, A., Tavman, I. H., Chirtoc, M., … Novak, I. (2016). Effect of aspect ratio on thermal conductivity of high density polyethylene/multi-walled carbon nanotubes nanocomposites. *Composites Part A: Applied Science and Manufacturing*, *82*, 208–213.

Fontes, D. H., Ribatski, G., & Bandarra Filho, E. P. (2015). Experimental evaluation of thermal conductivity, viscosity and breakdown voltage AC of nanofluids of carbon nanotubes and diamond in transformer oil. *Diamond and Related Materials*, *58*, 115–121.

Hashim, D. P., Narayanan, N. T., Romo-Herrera, J. M., Cullen, D. A., Hahm, M. G., Lezzi, P., … Ajayan, P. M. (2012). Covalently bonded three-dimensional carbon nanotube solids via boron induced nanojunctions. *Scientific Reports*, *2*, 363.

Hilding, J., Grulke, E. a., George Zhang, Z., & Lockwood, F. (2007). Dispersion of Carbon Nanotubes in Liquids. *Journal of Dispersion Science and Technology*, *24*(1), 1–41.

Hoffmann, J. F., Henry, J. F., Vaitilingom, G., Olives, R., Chirtoc, M., Caron, D., & Py, X. (2016). Temperature dependence of thermal conductivity of vegetable oils for use in concentrated solar power plants, measured by 3omega hot wire method. *International Journal of Thermal Sciences*, *107*, 105–110.

Horinek, D. (2014). DLVO Theory. In G. Kreysa, K. Ota, & R. F. Savinell (Eds.), *Encyclopedia of Applied Electrochemistry* (343–346). New York, NY: Springer New York.

Huang, T.-C., Li, P., Yao, H., Sue, H.-J., Kotaki, M., & Tsai, M. (2016). Highly efficient oil-water separators based on dual superhydrophobic and superoleophilic properties of multiwall-carbon nanotube filtration films. *Rsc Advances*, *6*(15), 12422–12425.

Hunter, R. J. (2001). *Foundations of colloid science*. Oxford University Press.

Hwang, Y., Lee, J. K., Lee, C. H., Jung, Y. M., Cheong, S. I., Lee, C. G., … Jang, S. P. (2007). Stability and thermal conductivity characteristics of nanofluids. *Thermochimica Acta*, *455*(1–2), 70–74.

Hwang, Y., Park, H. S., Lee, J. K., & Jung, W. H. (2006). Thermal conductivity and lubrication characteristics of nanofluids. *Current Applied Physics*, *6*(SUPPL. 1), 67–71.

Ilyas, S. U., Pendyala, R., & Narahari, M. (2017). Stability and thermal analysis of MWCNT-thermal oil-based nanofluids. *Colloids and Surfaces A: Physicochemical and Engineering Aspects*, *527*(March), 11–22.

Jang, W., Bao, W., Jing, L., Lau, C. N., Dames, C., Jang, W., … Dames, C. (2015). Thermal conductivity of suspended few-layer graphene by a modified T-bridge method, *133102*(2013), 1–6.

John, G. (1997). Richard Feynman: A life in science. *Dutton, NY*, *170*.

Kayvani Fard, A., Mckay, G., Manawi, Y., Malaibari, Z., & Hussien, M. A. (2016). Outstanding adsorption performance of high aspect ratio and super-hydrophobic carbon nanotubes for oil removal. *Chemosphere*, *164*, 142–155.

Kim, P., Shi, L., Majumdar, A., & McEuen, P. L. (2001). Thermal Transport Measurements of Individual Multiwalled Nanotubes. *Physical Review Letters*, *87*(21), 215502.

Kommandur, S., Mahdavifar, A., Jin, S., Hesketh, P. J., & Yee, S. (2016). Sensors and Actuators A : Physical Metal-coated glass microfiber for concentration detection in gas mixtures using the 3-Omega excitation method. *Sensors & Actuators: A. Physical*, *250*, 243–249.

Kreith, F., Manglik, R. M., & Bohn, M. S. (2012). *Principles of Heat Transfer, SI Edition*. Cengage Learning. Retrieved September 26, 2017, from https://books.google.com.tr/books?id=2TYKAAAAQBAJ

Lee, C. H., Johnson, N., Drelich, J., & Yap, Y. K. (2011). The performance of superhydrophobic and superoleophilic carbon nanotube meshes in water-oil filtration. *Carbon*, *49*(2), 669–676.

Lee, K., Hwang, Y., Cheong, S., Kwon, L., Kim, S., & Lee, J. (2009). Performance evaluation of nano-lubricants of fullerene nanoparticles in refrigeration mineral oil. *Current Applied Physics*, *9*(2 SUPPL.), e128–e131.

Li, Q., Church, J. S., Kafi, A., Naebe, M., & Fox, B. L. (2014). An improved understanding of the dispersion of multi-walled carbon nanotubes in non-aqueous solvents. *Journal of Nanoparticle Research*, *16*(7).

Liu, M.-S., Ching-Cheng Lin, M., Huang, I.-T., & Wang, C.-C. (2005). Enhancement of thermal conductivity with carbon nanotube for nanofluids. *International Communications in Heat and Mass Transfer*, *32*(9), 1202–1210.

Liu, M., Lin, M. C., & Wang, C. (2011). Enhancements of thermal conductivities with Cu, CuO, and carbon nanotube nanofluids and application of MWNT/water nanofluid on a water chiller system. *Nanoscale Research Letters*, *6*(1), 297.

Ma, P. C., Siddiqui, N. A., Mäder, E., & Kim, J. K. (2011). Correlation between electrokinetic potential, dispersibility, surface chemistry and energy of carbon nanotubes. *Composites Science and Technology*, *71*(14), 1644–1651.

Marquis, F. D. S., & Chibante, L. P. F. (2005). Improving the Heat Transfer of Nanofl uids and Nanolubricants with Carbon Nanotubes. *JOM*, *d*(December), 2005.

Masuda, H., Ebata, A., Teramae, K., & Hishinuma, N. (1993). Alteration of Thermal Conductivity and Viscosity of Liquid by Dispersing Ultra-Fine Particles. *Netsu Bussei*, *7*(4), 227–233.

Munkhbayar, B., Nine, M. J., Hwang, S., Kim, J., Bae, K., Chung, H., & Jeong, H. (2012). Effect of grinding speed changes on dispersibility of the treated multi-walled carbon nanotubes in aqueous solution and its thermal characteristics. *Chemical Engineering and Processing: Process Intensification*, *61*, 36–41.

Nadolny, Z., Dombek, G., & Przybylek, P. (2016). Thermal properties of a mixture of mineral oil and synthetic ester in terms of its application in the transformer. *Annual Report - Conference on Electrical Insulation and Dielectric Phenomena, CEIDP*, *2016–Decem*, 857–860.

O'Driscoll, L. J., Welsh, D. J., Bailey, H., Bryce, M. R., & Lambert, C. J. (2014). Reversible thermal switching of aqueous dispersibility of multiwalled carbon nanotubes. *Chemistry - A European Journal*, *21*(10), 3891–3894.

Paolucci, S., Puliti, G., Paolucii, S., & Puliti, G. (2015). *Properties of Nanofluid*. *Heat transfer Enhancement wirh Nanofluids*. CRC.

Paul, G., Chopkar, M., Manna, I., & Das, P. K. (2010). Techniques for measuring the thermal conductivity of nanofluids: A review. *Renewable and Sustainable Energy Reviews*, *14*(7), 1913–1924.

Shaikh, S., Lafdi, K., & Ponnappan, R. (2007). Thermal conductivity improvement in carbon nanoparticle doped PAO oil: An experimental study. *Journal of Applied Physics*, *101*(6).

Soulie-Ziakovic, C., Nicolay, R., Prevoteau, A., & Leibler, L. (2014). Dispersible carbon nanotubes. *Chemistry - A European Journal*, *20*(5), 1210–1217.

Tantra, R., Schulze, P., & Quincey, P. (2010). Effect of nanoparticle concentration on zeta-potential measurement results and reproducibility. *Particuology*, *8*(3), 279–285.

Tian, L., Li, Y., Webb, R. C., Krishnan, S., Bian, Z., Song, J., … Rogers, J. A. (2017). Flexible and Stretchable 3 ω Sensors for Thermal Characterization of Human Skin, *1701282*, 1–9.

Turgut, A., Sauter, C., Chirtoc, M., Henry, J. F., Tavman, S., Tavman, I., & Pelzl, J. (2008). AC hot wire measurement of thermophysical properties of nanofluids with 3ω method. *European Physical Journal: Special Topics*, *153*(1), 349–352.

Turgut, A., Tavman, I., Chirtoc, M., Schuchmann, H. P., Sauter, C., & Tavman, S. (2009). Thermal conductivity and viscosity measurements of water-based TiO 2 nanofluids. *International Journal of Thermophysics*, *30*(4), 1213–1226.

Vakili-Nezhaad, G. R., & Dorany, A. (2009). Investigation of the Effect of Multiwalled Carbon Nanotubes on the Viscosity Index of Lube Oil Cuts. *Chemical Engineering Communications*, *196*(9), 997–1007.

Wang, H. J., Ma, S. J., Yu, H. M., Zhang, Q., Guo, C. M., & Wang, P. (2014). Thermal conductivity of transformer oil from 253 k to 363 K. *Petroleum Science and Technology*, *32*(17), 2143–2150.

Wang, J. J., Zheng, R. T., Gao, J. W., & Chen, G. (2012). Heat conduction mechanisms in nanofluids and suspensions. *Nano Today*, *7*(2), 124–136.

Wang, Z. L., Tang, S., & Araki, N. (2007). Thermal-conductivity and thermal-diffusivity measurements of nanofluids by 3ω method and mechanism analysis of heat transport. *International Journal of Thermophysics*, *28*(4), 1255–1268.

Wei, Y., Ling, X., Zou, L., Lai, D., Lu, H., & Xu, Y. (2015). A facile approach toward preparation of sulfonated multi-walled carbon nanotubes and their dispersibility in various solvents. *Colloids and Surfaces A: Physicochemical and Engineering Aspects*, *482*, 507–513.

Wu, Z., & Mitra, S. (2014). Length reduction of multi-walled carbon nanotubes via high energy ultrasonication and its effect on their dispersibility. *Journal of Nanoparticle Research*, *16*(8).

Xie, H., Lee, H., Youn, W., & Choi, M. (2003). Nanofluids containing multiwalled carbon nanotubes and their enhanced thermal conductivities. *Journal of Applied Physics*, *94*(8), 4967–4971.

Yang, B., & Han, Z. H. (2006). Temperature-dependent thermal conductivity of nanorod-based nanofluids. *Applied Physics Letters*, *89*(8), 3–6.

Yang, K., Yi, Z. L., Jing, Q. F., Yue, R. L., Jiang, W., & Lin, D. H. (2013). Sonication-assisted dispersion of carbon nanotubes in aqueous solutions of the anionic surfactant SDBS: The role of sonication energy. *Chinese Science Bulletin*, *58*(17), 2082–2090.

Yang, Y., Grulke, E. A., Zhang, Z. G., & Wu, G. (2006). Thermal and rheological properties of carbon nanotube-in-oil dispersions. *Journal of Applied Physics*, *99*(11).

Zhang, X., Liu, M., Zhang, X., Deng, F., Zhou, C., Hui, J., … Wei, Y. (2015). Interaction of tannic acid with carbon nanotubes: enhancement of dispersibility and biocompatibility. *Toxicology Research*, *4*(1), 160–168.